

# Explosion Mechanisms of Core-Collapse Supernovae

Hans-Thomas Janka

*Max Planck Institute for Astrophysics, Karl-Schwarzschild-Str. 1,  
D-85748 Garching, Germany; email: thj@mpa-garching.mpg.de*

Supernova theory, numerical and analytic, has made remarkable progress in the past decade. This progress was made possible by more sophisticated simulation tools, especially for neutrino transport, improved microphysics, and deeper insights into the role of hydrodynamic instabilities. Violent, large-scale nonradial mass motions are generic in supernova cores. The neutrino-heating mechanism, aided by nonradial flows, drives explosions, albeit low-energy ones, of ONeMg-core and some Fe-core progenitors. The characteristics of the neutrino emission from new-born neutron stars were revised, new features of the gravitational-wave signals were discovered, our notion of supernova nucleosynthesis was shattered, and our understanding of pulsar kicks and explosion asymmetries was significantly improved. But simulations also suggest that neutrino-powered explosions might not explain the most energetic supernovae and hypernovae, which seem to demand magnetorotational driving. Now that modeling is being advanced from two to three dimensions, more realism, new perspectives, and hopefully answers to long-standing questions are coming into reach.

Keywords: massive stars — neutrinos — hydrodynamics — magnetic fields — neutron stars — black holes

## I. INTRODUCTION: ROOTS AND QUESTIONS

When, why, and how can the catastrophic infall of the core of a massive star be reversed to trigger the powerful ejection of the stellar mantle and envelope in a supernova (SN) explosion? This fundamental problem of stellar astrophysics has been a matter of intense research since the crucial role of SNe for the synthesis of heavy elements and for the dissemination of the nuclear burning products of stars had been recognized by Burbidge et al. [1]. The latter authors also noticed that nuclear statistical equilibrium in the hot, dense core of evolved stars (at  $T \gtrsim 7 \times 10^9$  K) favors iron dissociation to alpha particles, and they concluded that the huge demand of energy (about 1.7 MeV per nucleon or  $1.7 \times 10^{18}$  erg per gram) must be supplied by gravitational binding energy, leading to a contraction of the stellar core and ultimately to a dynamical implosion on a timescale of less than a second,  $t_{\text{coll}} \sim 0.21/\sqrt{\rho_8}$  s, when the average density  $\rho_8 \equiv \rho/(10^8 \text{ g/cm}^3)$  exceeds unity. This groundbreaking insight is in line with Baade & Zwicky's earlier idea that SNe could represent the transition of ordinary stars to neutron stars (NSs) [2].

Already in 1960 Hoyle & Fowler [3] proposed the two basic scenarios of stellar death: thermonuclear runaway at degenerate conditions (which, as we know now, drives the destruction of white dwarf stars in Type Ia SNe) and the implosion of stellar cores (associated with what is called core-collapse supernovae (CCSNe) of Types II, Ib/c, and hypernovae<sup>1</sup>). They hypothesized (following [1]) that the gravitational compression of the core raises the temperature such that thermonuclear fuel could be ignited to release the energy for triggering the ejection of the outer parts of the star. They also mentioned simulations by Colgate & Johnson [4, 5], in which the “bounce” of a forming NS launched a spherical shock wave that reversed the infall of the overlying stellar shells to make them gravitationally unbound. Colgate & White [6] realized that gravitational binding energy of order  $E_b \sim GM_{\text{ns}}^2/R_{\text{ns}} > 10^{53}$  erg, which is released when the core of a star collapses to a NS, is converted to neutrino emission and provides a huge energy reservoir for powering the SN blast wave. They argued correctly that in stellar layers pulled inward at supersonic speed along with the imploding core, thermonuclear combustion is unable to initiate an outward acceleration. Instead they proposed that a fraction of the intense neutrino flux may get absorbed in the mantle of the star to cause the explosion.

More than four decades of theoretical and numerical modeling work, spearheaded by early pioneers of the field like Dave Arnett, Jim Wilson, Hans Bethe, Gerry Brown, Steve Bruenn, Wolfgang Hillebrandt, Jim Lattimer, and David Schramm, have helped to sharpen our picture of the diverse physical ingredients and processes that play a role in the core of dying stars, among them magnetohydrodynamic (MHD) effects, fluid instabilities and turbulent flows, the finite-temperature equation of state (EoS) of NS matter, neutrino transport and neutrino-matter interactions, and

<sup>1</sup> Observationally, SNe II exhibit strong H-Balmer lines in their early spectra, whereas SNe I show no H-lines. In SNe Ia there are Si-lines, in SNe Ib no Si- but He-lines, and in SNe Ic none of these, indicating explosions of stars that had lost their hydrogen envelope or both the outer hydrogen and helium shells before collapse. More sub-classes have been introduced, some of them motivated only by recent discoveries: SNe II-P and II-L are discriminated by a plateau phase or linear decay of their lightcurves after the peak, IIb events have only thin H-shells left, and spectra of IIa and IIn cases possess signatures of a dense circumstellar medium.

general relativistic gravity. While the bounce-shock mechanism is not supported by any modern simulation with state-of-the-art treatment of the physics, the “delayed neutrino-heating mechanism” as discussed by Bethe and Wilson [7] and aided by violent, nonradial mass motions in the collapsing stellar core [8–11], has advanced to the widely favored scenario for powering the majority of SNe.

The momentum behind the quest for solving the puzzle of the SN mechanism originates from important questions at the interface of astrophysics and nuclear, particle, and gravitational physics, for example:

- What is the link between the properties of SNe and their progenitor stars?
- Which stars collapse to black holes (BHs) instead of NSs, which fraction of stellar collapses do not yield explosions?
- What are the birth properties of the compact remnants, i.e. their masses, spins, magnetic fields, and recoil velocities?
- How can the high velocities of young pulsars be explained? Is any exotic physics necessary?
- What characteristics does the neutrino burst from a SN have and what does it tell us about neutrino properties and the extreme conditions in the newly formed NS?
- What is the gravitational-wave signature of a stellar collapse event and which information can we extract about the dynamical processes in the SN core?
- What is the nucleosynthetic role of massive star explosions in the chemogalactic history?
- Are SNe the long-sought sources of r-process elements, in particular also of the lanthanides, the third abundance peak, and actinides?
- What is the population-integrated energetic footprint left by SN explosions in the dynamical evolution of galaxies?

In the following sections we will review the known types of stellar collapse events (Sect. II), the ingredients and current status of numerical modeling (Sect. III), the mechanisms by which massive stars might explode (Sect. IV), and the signatures of the explosion mechanism that might serve for observational diagnostics (Sects. V and VI). We will provide an update of recent developments as follow-up and supplement of previous reports that have approached the topic from different perspectives [12–19].

## II. ROUTES TO STELLAR CORE COLLAPSE

Massive stars possess finite lifetimes of millions to tens of millions of years, which are mainly determined by the period the star spends on the main sequence (MS) during central hydrostatic hydrogen burning. The evolution time of stars scales approximately like  $t_{\text{evol}} \approx 7.3 \times 10^9 \text{ yr} (M_*/M_\odot)/(L_*/L_\odot)$  with the stellar mass  $M_*$  and luminosity  $L_*/L_\odot \approx (M_*/M_\odot)^{3.5}$  (where  $M_\odot = 1.989 \times 10^{33} \text{ g}$  and  $L_\odot = 3.85 \times 10^{33} \text{ erg/s}$  are solar mass and luminosity). When hydrogen in the stellar core gets exhausted and the star leaves the MS, its evolution speeds up considerably because the efficiency of energy production in the higher stages of nuclear burning decreases and concurrently energy losses through neutrino-antineutrino pairs rise dramatically. This is the case in particular when the central temperature of the star climbs to  $T_c \sim 10^9 \text{ K}$ , at which time  $e^+e^-$  pairs become abundant and the energy drain in  $\nu\bar{\nu}$  pairs accelerates with  $T_c^9$ . At this time neutrino losses exceed the radiation losses of the star and the evolution of the helium core decouples from that of the stellar envelope.

The energy drain happens at the expense of gravitational binding, leading to continuous contraction of the stellar core, which is slowed down only temporarily by the periods of nuclear burning. As long as nondegenerate particles dominate the pressure of the stellar plasma, hydrostatic equilibrium requires that the central temperature,  $T_c$ , and central density,  $\rho_c$ , roughly follow the proportionality

$$\frac{T_c^3}{\rho_c} \propto M_c^2 \sim \text{const} . \quad (1)$$

According to this relation more massive stars with bigger He-cores (larger  $M_c$ ) are hotter (Fig. 1). For sufficiently high central temperature, nuclear fuel can ignite in the next burning stage, building up heavier and more stable

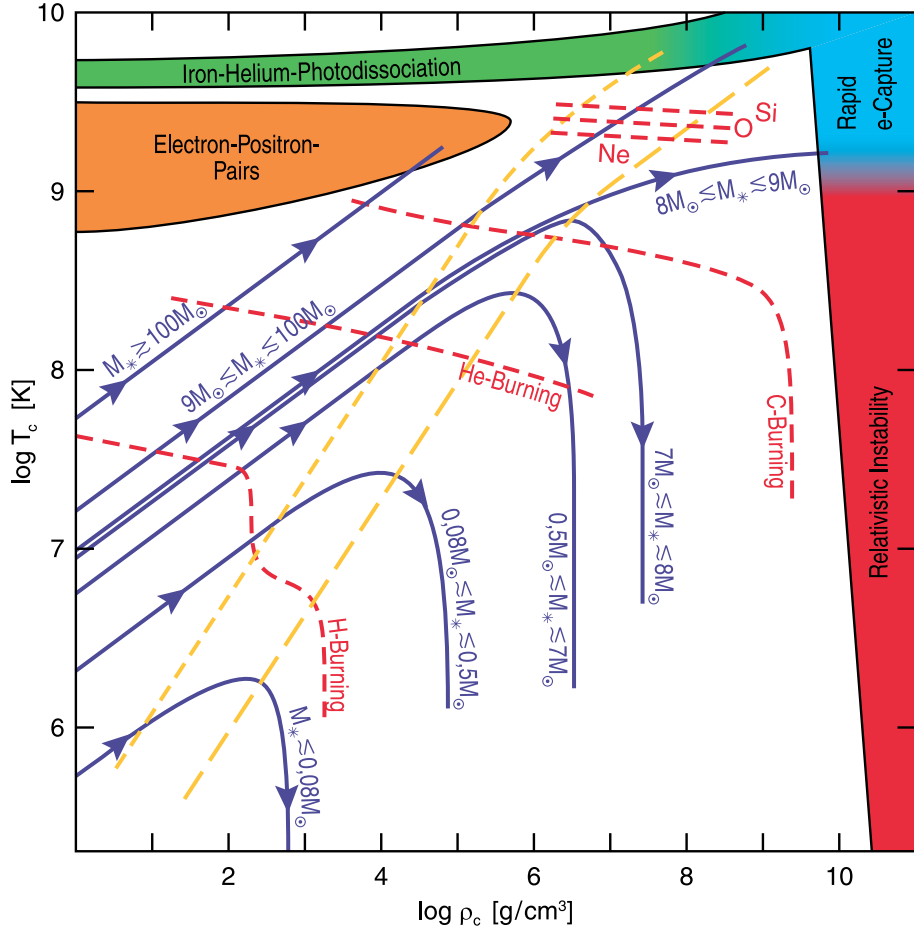


FIG. 1: Stellar death regions with schematic stellar evolution tracks in the plane of central density ( $\rho_c$ ) and central temperature ( $T_c$ ). Colored death regions are labeled by the instability process causing the collapse of the stellar core, and the blue tracks are labeled by the corresponding rough birth-mass range of objects reaching the different stages of central burning (indicated by red dashed lines). Yellow diagonal lines mark the beginning of degeneracy (short-dashed) and strong degeneracy (long-dashed) of the electron plasma. Note that realistic stellar tracks exhibit wiggles and loops when the ignition of the next burning stage is reached and the stellar core adjusts to the new energy source (see Ref. [20]).

elements in their inner core. If, however, the stellar interior enters the regime of electron degeneracy before<sup>2</sup> (yellow, short-dashed line in Fig. 1) it ends as a white dwarf, being stabilized by lepton degeneracy pressure and cooling at essentially fixed density.

Stars beyond certain birth-mass limits can reach the “death zones” in the upper and right parts of Fig. 1, where the stellar core becomes gravitationally unstable. Contraction, and in the case of a runaway process finally collapse, sets in when the effective adiabatic index drops below the critical value of  $4/3$  for mechanical stability (the actual value is slightly decreased by rotation and increased by general relativistic gravity).

Three different processes can initiate the implosion of stellar cores in three areas of the  $\rho_c$ - $T_c$ -plane indicated by different colors in Fig. 1, playing a role in different kinds of CC events.

<sup>2</sup> Fermions approach the degeneracy when their Fermi energy begins to exceed the thermal energy  $k_B T$ , i.e. at  $T_8 \sim 4\rho_5^{2/3}$  for nonrelativistic electrons and at  $T_{10} \sim \rho_8^{1/3}$  for relativistic ones with  $T_x \equiv T/(10^x \text{ K})$  and  $\rho_y \equiv \rho/(10^y \text{ g cm}^{-3})$ .

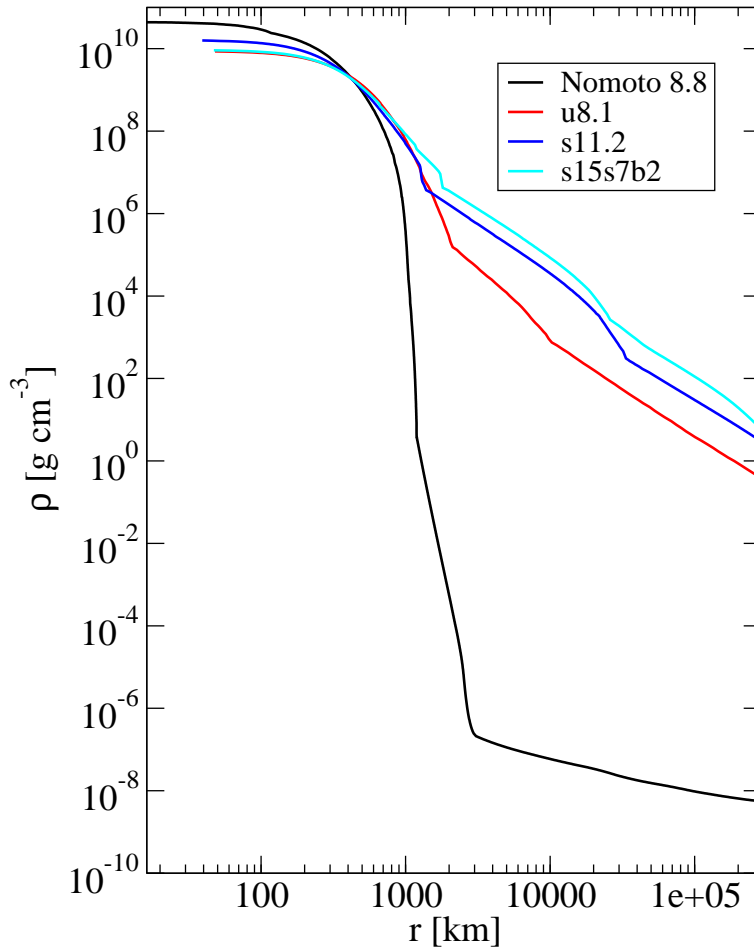


FIG. 2: Core-density profiles of different SN progenitors at the onset of gravitational collapse. The black line corresponds to the ONeMg core of an  $8.8 M_{\odot}$  star [21], the other three are SN progenitors with iron cores: an  $8.1 M_{\odot}$  ultra metal-poor ( $10^{-4}$  solar metallicity) star (A. Heger, private communication) and  $11.2 M_{\odot}$  [22] and  $15 M_{\odot}$  [23] solar-metallicity stars. The steps and kinks in the curves correspond to composition-shell interfaces (Fe/Si and O/C for the  $11.2$  and  $15 M_{\odot}$  models and inner and outer boundaries of a C-O-Ne-layer for the  $8.1 M_{\odot}$  case).

### A. Electron-Capture Supernovae

The lowest-mass progenitors of CCSNe develop oxygen-neon-magnesium (ONeMg) cores through C-burning [21, 28, 29] but reach  $e$ -degeneracy before hydrostatic Ne-burning can be ignited. Due to low reaction thresholds of Ne and Mg, the increasing electron Fermi energy enables  $e$ -captures (right upper corner of Fig. 1), triggering gravitational collapse and resulting in an electron-capture SN (ECSN). Solar-metallicity stars<sup>3</sup> with  $9$ – $9.25 M_{\odot}$  are estimated to have that destiny [29], but the mass window is expected to shift and widen for lower metallicities [30] and in binary systems with mass loss or transfer [31] so that ECSNe could contribute even 20–30% of all SNe [32, 33].

Because of the extremely steep density decline in a thin C-O-shell ( $\sim 0.1 M_{\odot}$  between about  $3 \times 10^4 \text{ g/cm}^3$  and  $4 \times 10^8 \text{ g/cm}^3$ ) at the edge of the O-Ne core (Fig. 2), these stars have special explosion properties (Sect. IV C). They eject little carbon and oxygen and very little nickel, their SNe will therefore be relatively faint. The Crab remnant of SN 1054 is thought to be the relic of such an explosion [34, 35], and an increasing number of dim events like SN 1997D, 1999br, 2005cs, 2008S and other recently observed transient sources are discovered as possible candidates.

<sup>3</sup> The metallicity  $Z$  is the total mass fraction of chemical elements heavier than helium in the matter the star was formed of. The solar value has been determined to be 0.016.

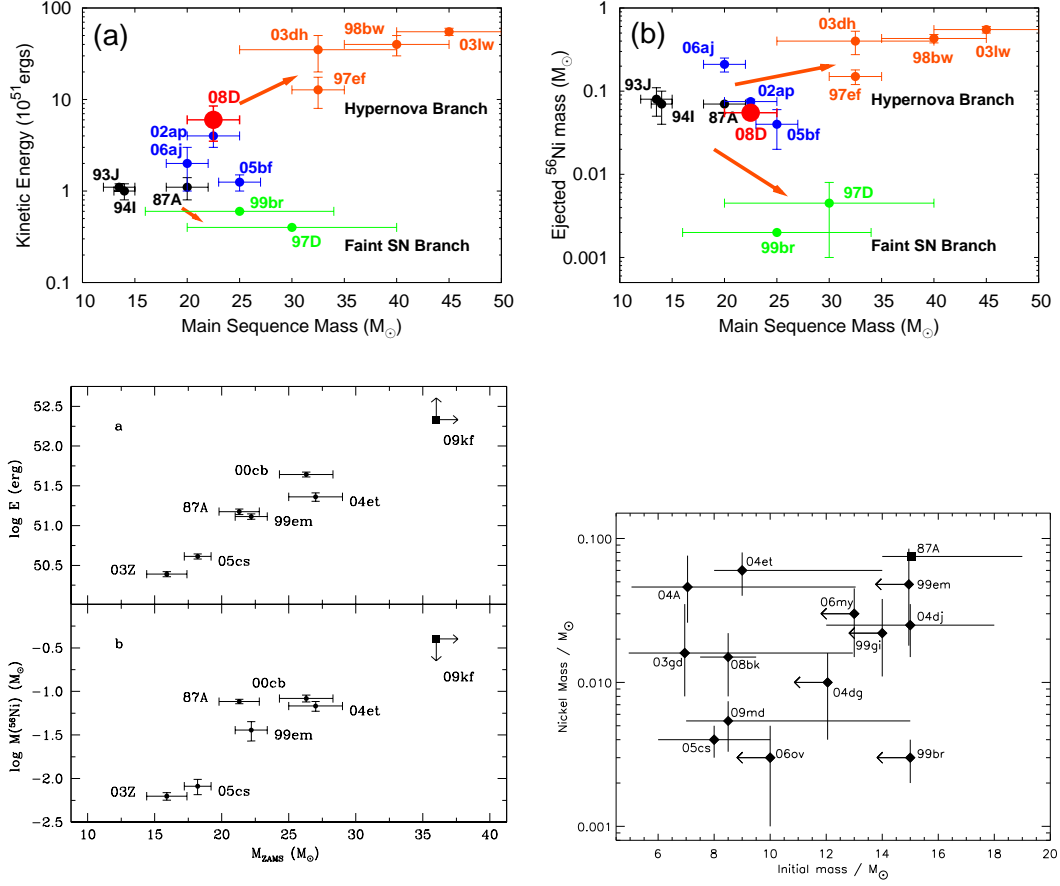


FIG. 3: Kinetic energies and ejected nickel masses for stellar explosions versus initial (zero-age main sequence; ZAMS) masses from different authors. While explosion properties are deduced from comparing observations with lightcurve and spectra calculations based on (spherically symmetric) models, the ZAMS masses are estimated by linking ejecta masses to initial masses through stellar evolution models with mass-loss assumptions (*upper panels* [24] and *lower left panel* [25]; reproduced by permission of the authors and AAS and ©ESO, respectively) or by inferring ZAMS masses or upper limits from computed stellar evolution histories that account for the properties of discovered SN progenitors or their stellar environments (i.e., coeval star clusters, host galaxies [26, 27]; *lower right panel*, kindly provided by John Eldridge and Stephen Smartt). Due to theoretical uncertainties this leads to largely different mass determinations for some cases (SN 1987A, SN 1999br, SN 1999em, SN 2004et, SN 2005cs). For masses  $\gtrsim 25 M_{\odot}$  Tanaka et al. [24] discriminated a very energetic and bright HN branch from a low-energy, faint SN branch. The objects with little nickel production of the latter branch, however, have also been interpreted as weak explosions (possibly ECSNe) near the lower mass limit for SN progenitors.

## B. Iron-Core Supernovae

Massive stars that ignite hydrostatic Ne-burning form an iron core. The latter becomes gravitational unstable when the nuclear statistical equilibrium (NSE) at temperatures around  $10^{10}$  K ( $k_{\text{B}}T \sim 1$  MeV) favors the dissociation of iron-group nuclei to  $\alpha$ -particles and a growing number of free nucleons (upper region in Fig. 1). With the onset of contraction and increasing density and electron chemical potential, also  $e$ -captures on nuclei (and some free protons) speed up and accelerate the implosion. The dynamical collapse is abruptly stopped only when nuclear densities ( $\rho \gtrsim 2.7 \times 10^{14}$  g/cm $^3$ ) are reached, and the phase transition to homogeneous nuclear matter leads to a sudden increase of the effective adiabatic index due to repulsive short-range forces between nucleons.

When the overshooting inner core rebounds and crashes supersonically into the subsequently infalling layers, sound waves steepen into a shock front that ultimately leads to the disruption of the star in the SN explosion. However, different from ONeMg cores, the much flatter density profile in and around Fe cores (Fig. 2) leads to long-lasting, high mass accretion rates and large ram pressure of the infalling shells. This impedes the outward propagation of the shock and makes Fe-core progenitors harder to blow up than stars with ONeMg core. Although more massive stars exhibit a gross tendency to bigger He-cores and shallower density decline, the variation with stellar birth mass is not

necessarily monotonic [22]. The mechanism(s) by which ECSNe and Fe-core SNe succeed to explode will be discussed in Sect. IV.

Stellar cores of pre-SN stars are expected to rotate relatively slowly, i.e. with average pre-collapse spin periods of tens of seconds or more. This is a consequence of angular momentum loss associated with mass loss phases (in particular when the star becomes a red giant), because magnetic torques from fields generated by differential rotation in the star couple core and envelope and thus transport angular momentum efficiently out of the core [36]. Stellar rotation is therefore not expected to play a crucial role for the explosion mechanism of normal CCSNe (Sect. IV D).

### C. Gamma-Ray Burst Supernovae

Rapid stellar rotation, however, is thought to be crucial in the case of gamma-ray burst (GRB) SNe and hypernovae (HNe) (for a review, see [15]). The latter originally obtained their name because of exceptional brightness and thus high nickel production [37] but are now considered as stellar explosions with unusually high ejecta velocities (i.e., very broad spectral lines) and thus large kinetic energies [38] (Fig. 3). HNe are found to be associated with long-duration ( $t_{\text{GRB}} \gtrsim 2$  s) GRBs, either observed spectroscopically (e.g., SN 1998bw with GRB 980425, SN 2003dh with GRB 030329, SN 2003lw with GRB 031203, SN 2006aj with GRB 060218, SN 2010bh with GRB 100316D) or as late lightcurve humps superimposed on the power-law decline of the afterglow that follows the GRB.

GRBs with their extremely luminous high-energy radiation are understood as ultrarelativistic, collimated outflows (“jets”). Strong global asymmetry is also suggested by line profiles (in particular double-peaked oxygen emission lines) seen in many HNe. Such events are interpreted as signatures of BH-forming stellar collapses (“collapsars” [39]), in which matter around a rapidly spinning BH is able to set free energy in neutrinos, electromagnetic poynting flux, and mass outflow with an efficiency of up to roughly 40% of the rest-mass energy of accreted material,  $\dot{E}_{\text{acc}} \lesssim 0.4 \dot{M} c^2 \sim 10^{54} (\dot{M}/M_{\odot}/\text{s}) \text{ erg/s}$ . Alternatively, a nearly critically rotating NS,  $t_{\text{rot}} \sim 1$  ms, with ultrastrong dynamo-generated magnetic field,  $\langle B \rangle \gtrsim 10^{15}$  G, (“millisecond magnetar”) is discussed as possible central engine of GRBs and HNe. The jet and stellar explosion could either be powered by rotational energy of the magnetar or by gravitational and rotational energy of the accretion flow and BH. Both can be tapped by magnetic fields through MHD effects (Sect. IV D) and by neutrinos radiated from matter heated by magnetically generated viscous dissipation [40]. The existence of expected strong disk “winds” with the observed large Ni production [15], however, seems to be challenged by MHD simulations [41].

The progenitors of collapsars and GRB-HNe are thought to possess a massive core, which forms a BH instead of exploding before. They must be compact stars without an extended hydrogen envelope in order to allow jets to emerge ultrarelativistically, i.e., the crossing time of the jet must be shorter than the on-time of the central engine:  $R_*/c \lesssim t_{\text{engine}}$ . Moreover, the collapsing stellar core must contain a high specific angular momentum,  $j \gtrsim GM_{\text{BH}}/c \gtrsim 10^{16} M_{\text{BH}}/(3 M_{\odot}) \text{ cm}^2/\text{s}$ , to either form a magnetar with the necessary huge reservoir of rotational energy or to allow for a thick, massive accretion disk that remains long enough around the newly formed BH to efficiently release energy.

Such requirements favor rapidly rotating Wolf-Rayet stars as progenitors, but special initial conditions (a high birth spin) and evolution paths avoiding combined mass and angular momentum loss, or alternatively binary scenarios, are necessary [42, 43]. In the present-day universe HNe and GRB-SNe are rare (with a GRB/SN ratio of  $\sim 1/1000$ , less than 1% of all SN Ib/c produce GRBs), but BH-forming CC events and GRBs could be very common in the early (metallicity less than  $\sim 1/10$  solar) universe. This theoretical expectation is compatible with the fact that GRB-SNe are preferentially (but not exclusively) observed in low-metallicity environments.

### D. Pair-Instability Supernovae

Stars above about  $100 M_{\odot}$  are very hot and encounter the pair instability (in the upper left corner of Fig. 1) after central carbon burning (e.g., [22, 44] and refs. therein) at  $T \sim 10^9$  K. The gravitational instability occurs because the formation of  $e^+e^-$  pairs from high-energy photons converts thermal energy to rest-mass energy and thus reduces the adiabatic index of the EoS below  $4/3$ .

In the stellar mass range between  $\sim 100 M_{\odot}$  and  $\sim 140 M_{\odot}$  and for  $M_* \gtrsim 260 M_{\odot}$  collapse to a BH is expected. For intermediate masses the ignition of the still available thermonuclear fuel during the implosion is violent enough to trigger the complete disruption of the star with an explosion energy up to more than  $10^{53}$  erg and the production of up to  $\gtrsim 50 M_{\odot}$  of  $^{56}\text{Ni}$  [22, 44]. While such “thermonuclear core-collapse SNe” were originally termed “hypernovae” by Woosley & Weaver [45], they are now commonly called pair-instability SNe (PISNe) or pair-capture SNe (PCSNe). In the case of BH formation, in particular in the presence of rotation allowing for an accretion torus, huge amounts of energy are released in neutrinos, roughly  $(0.01\text{--}0.03) M_* c^2 \sim 10^{55}$  erg, depending on the angular momentum [46].

TABLE I: Neutrino reactions with stellar-medium particles and between neutrinos in the Garching models.  $N$  means either  $n$  or  $p$ ,  $\nu \in \{\nu_e, \bar{\nu}_e, \nu_\mu, \bar{\nu}_\mu, \nu_\tau, \bar{\nu}_\tau\}$ , and  $\nu_x \in \{\nu_\mu, \bar{\nu}_\mu, \nu_\tau, \bar{\nu}_\tau\}$ . In addition to “inelastic” nucleon recoil, thermal motions, phase-space blocking, high-density  $N$ - $N$ -correlations [51] and weak magnetism corrections [52], also quenching of the axial-vector coupling [53] and the reduction of the effective nucleon mass at high densities [54] are taken into account in the rates marked with a dagger ( $^\dagger$ ). A prime indicates that the neutrino can exchange energy with the scattering target (non-conservative or “inelastic” scattering)

Process	References
Beta-Processes	
$\nu_e + n \rightleftharpoons e^- + p$	[51] $^\dagger$
$\bar{\nu}_e + p \rightleftharpoons e^+ + n$	[51] $^\dagger$
$\nu_e + (A, Z) \rightleftharpoons e^- + (A, Z + 1)$	[55]
Scattering Reactions	
$\nu + (A, Z) \rightleftharpoons \nu' + (A, Z)$	[56] (ion-ion correlations)
	[57] (inelastic contribution)
$\nu + N \rightleftharpoons \nu' + N$	[51] $^\dagger$
$\nu + e^\pm \rightleftharpoons \nu' + e^\pm$	[58]
(“Thermal”) Pair Production	
$\nu + \bar{\nu} \rightleftharpoons e^- + e^+$	[59, 60]
Nucleon-Nucleon Bremsstrahlung	
$\nu + \bar{\nu} + N + N \rightleftharpoons N + N$	[61]
Reactions between Neutrinos	
$\nu_{\mu,\tau} + \bar{\nu}_{\mu,\tau} \rightleftharpoons \nu_e + \bar{\nu}_e$	[62]
$\nu_x + \{\nu_e, \bar{\nu}_e\} \rightleftharpoons \nu'_x + \{\nu'_e, \bar{\nu}'_e\}$	[62]

While some recently discovered ultra-bright SNe and transients (for example SN 2002ic, 2005gj, 2005ap, 2006gy, 2007bi, 2008es, 2010gx) have been discussed as PISN candidates (e.g., [47, 48]), other explanations for the extreme luminosity than excessive Ni yields have been proposed, e.g., interaction of explosion ejecta with a dense circumstellar medium [49] or additional energy release by magnetar spin-down [50]. The expected rate of PISNe is small, maybe one of 100–1000 normal stellar core collapses, and presumably mostly associated with metal-poor host galaxies. In the Milky Way possibly two dozen very massive hypergiants like the evolved luminous blue variable star  $\eta$  Carinae might end their lives in such events.

Although the nature of the stellar death events associated with ultra-bright transients and in particular the energy source of their extraordinary luminosity are not at all clear and will remain a topic of intense research and debate in the coming years, space limitations demand to constrain the rest of this article mostly on the physics and processes that are relevant for the far majority of ordinary CCSNe.

### III. NUMERICAL MODELING AND PHYSICS INGREDIENTS

While over two decades that followed the pioneering work by Colgate & White [6], Arnett [63], and Wilson [64], SN modeling was constrained to spherically symmetric (1D) simulations with few exceptions only [65–68], the situation has radically changed in the post-SN 1987A era. Detailed observations of this nearest SN in the era of modern astronomy revealed that large-scale mixing processes had transported radioactive nuclei with velocities up to  $\sim 4000$  km/s from the deep core far into the hydrogen envelope of the exploding star, suggesting that spherical symmetry was broken already during the very first moments of the blast [69, 70]. Moreover, two-dimensional (2D) simulations in the early 1990s demonstrated that violent convective overturn takes place in the neutrino-heating layer between the gain radius and stalled accretion shock [8–11]. This raised hopes that buoyant energy transport to the shock could crucially support the delayed neutrino-heating mechanism and finally ensure robust explosions after 1D models had turned out to be successful only with special assumptions that could not withstand closer and more detailed analysis. For example, neutron-finger instability inside the nascent NS was proposed to enhance the neutrino luminosities and thus neutrino heating [71] but is disfavored because lepton equilibration between fingers and surroundings was shown to proceed faster than thermal equilibration [13, 72].

In the following sections more recent developments and the present status of numerical approaches will be briefly summarized. While three-dimensional (3D), general relativistic (magneto-)hydrodynamic simulations including mi-

microphysical EoS and sophisticated, energy-dependent neutrino transport are the ultimate, brave objective, only first steps have so far been achieved, approaching the goal from different directions. Mastering this grand computational challenge will require highly parallelized codes with excellent scaling capability on tens of thousands of processor cores to achieve sustained performance on the hundreds of teraflop/s to petaflop/s level. Still, one 3D model calculation will take a wall-clock time of several weeks to months.

### A. Hydrodynamics and Gravity

To date fully self-consistent modeling of stellar collapse and explosion in 3D has been achieved only by Fryer and collaborators [73–75], yet only by sacrificing many aspects which are important for quantitatively reliable and conclusive results concerning the SN mechanism. In particular, Newtonian gravity and a grey, flux-limited neutrino diffusion (FLD) scheme [8] were applied in combination with a smoothed particle hydrodynamics (SPH) method, which permits economical calculations in 3D with relatively low resolution but is noisy and diffusive. Good resolution and an accurate representation of the hydrodynamical quantities, however, are essential to treat the growth of fluid instabilities from initial seeds in the SN core [76, 77], and general relativity as well as a multi-group description of neutrino transport including velocity-dependent observer corrections were found to cause important differences in 1D [78, 79] and 2D simulations [80, 81].

Other groups, using mesh-based discretization schemes for solving the hydrodynamics, have so far studied only more constrained problems in 3D than [73–75], mostly also making even more radical approximations of the relevant (micro)physics. For example, in refs. [82, 83] the development of a nonradial hydrodynamic instability of the accretion shock in a collapsing stellar core, the so-called standing accretion shock instability (SASI; [84]), was investigated for a steady-state flow through outer and inner grid boundaries with an ideal-gas EoS and parametrized neutrino-cooling terms. In refs. [85, 86] a similar accretion setup was studied with a microphysical EoS and additional simple neutrino-heating terms for prescribed luminosities and spectra (neutrino “lightbulb” approximation, NLA), which enabled neutrino-driven convection. Using the NLA, refs. [87, 88] investigated the onset of an explosion in “realistic” collapsing stellar cores systematically by varying the driving neutrino luminosity to explore the dependence on the dimension (1D, 2D or 3D) of the simulation. Gravitational-wave (GW) signals from infall, core bounce, and early postbounce ( $\sim 100$  ms) phases were computed with 3D general relativity (GR) for NS and BH formation [89, 90] and with 3D Newtonian hydrodynamics and an effective general relativistic potential (developed as an approximation of GR gravity in [91, 92]) for NS formation [93], making various crude simplifications of the neutrino effects and partly even of the EoS of the stellar plasma.

A grey description of the neutrino transport outside of an excised high-density core of the proto-neutron star (PNS) according to ref. [94] was applied for exploring NS kicks, neutrino emission asymmetries, and GW signal characteristics by long-time 3D simulations of SN explosions in refs. [95, 96]. Very first results of Newtonian 3D calculations with more detailed multi-group (MG) transport treatments have already been put out, using “ray-by-ray” (RbR) MGFLD [97] or an implementation of the “isotropic diffusion source approximation” (IDSA, see Sect. III B) for  $\nu_e$  and  $\bar{\nu}_e$  with [98] or without [99] a RbR approach, coupled to a trapping treatment for heavy-lepton neutrinos.

### B. Neutrino Transport

Over the past decade sophisticated multi-energy group solvers for three-flavor neutrino transport including energy-bin coupling and velocity-dependent terms (corrections due to the motion of the stellar plasma) have been developed and applied to all stages of stellar core collapse and the transition to explosion in 1D calculations. On the one hand this was achieved by direct integration of the Boltzmann transport equation (BTE) with a discrete-ordinate ( $S_N$ ) method in GR simulations [100, 101], on the other hand by integrating the set of two-moment equations of the BTE for neutrino number, energy, and momentum using a variable Eddington-factor closure obtained from convergent iteration with a model (i.e. simplified) Boltzmann equation. The latter approach was developed for Newtonian [91, 102] as well as GR simulations [103]. It was also generalized for multi-dimensional applications by adopting a “ray-by-ray plus” (RbR+) approximation [80, 91], in which spherical transport problems are solved on each angular bin of a 2D or 3D polar coordinate grid. This approximation implies that the neutrino intensity is assumed to be axially symmetric around the radial direction and the neutrino flux is considered to be purely radial. The “plus” suffix signals, however, that neutrino pressure gradients and the lateral advection of neutrinos with fluid flows are taken into account in the optically thick regime to prevent artificial hydrodynamic instabilities [80].

All the published 1D and 2D SN models of the Garching group, e.g. in refs. [80, 104–107], include the full, state-of-the-art set of neutrino interactions listed in Table I. Recently, 1D results based on a similarly refined treatment of the neutrino processes have been put out by the Oak Ridge group [79].



Truely multi-dimensional, energy-dependent transport schemes for radiation-hydrodynamics with neutrinos have so far been used extensively in 2D Newtonian simulations only by the Arizona-Hebrew-Princeton collaboration, which applied a MGFLD method (e.g., in refs. [108–110]) and an  $S_N$  solver for a multi-angle (MA) treatment [111, 112], however without energy-bin coupling and without properly accounting for effects associated with fluid motions. This are severe shortcomings [79, 80], which are avoided in more elaborate 2D Newtonian implementations of MGFLD [113] and of a two-moment closure scheme for the coupled set of neutrino energy and momentum equations [114]. An alternative approach is the “isotropic diffusion source approximation” (IDSA; [115]), in which the neutrino distribution function is decomposed into trapped and streaming particle components, whose separate evolution equations are coupled by a diffusion source term. This method was simplified to a RbR version for  $\nu_e$  and  $\bar{\nu}_e$  and only a subset of neutrino processes in 2D [116] and 3D [98] SN simulations. A more detailed comparison and critical assessment of presently employed transport treatments can be found in ref. [79].

Pointing into the future, routes towards 3D time-dependent neutrino transport in radiation-hydrodynamics calculations have been outlined in the form of a rigorous solution of the 6+1 dimensional (three spatial dimensions, energy and two direction angles for the radiation momentum, plus time) BTE by an  $S_N$  discretization scheme [117], by spectral methods [118], and in GR by a truncated moment formalism [119], but observer corrections due to fluid motion, relativistic effects, nonlinear, energy-coupling interaction kernels, and high parallization efficiency are major challenges.

Direct comparisons of multi-dimensional SN calculations by different groups with different codes and approximations have not been carried out so far, in contrast to the 1D case [103, 120], and will be a formidable task for the coming years. However, FLD was shown to underestimate angular variations of the radiated neutrinos and to spheritize the radiation field compared to a multi-angle ( $S_N$ ) treatment [111], although fundamental changes of the hydrodynamic evolution were not observed despite higher neutrino-heating rates with the  $S_N$  code. On the contrary, the RbR approximation generically sharpens angular variations since all fluxes are radial. Local emission maxima (“hot spots”) in the neutrinospheric region therefore send radiation only in radial direction. Nevertheless, because nonspherical accretion flows in the SN core exhibit unsteady behavior in space and time (see, e.g., [96]) “variational averaging” can be expected to diminish any dynamical consequences of local emission peaks [80].

Despite undeniable weaknesses, the complexity and computational intensity of neutrino-hydrodynamics in full generality will make the use of simplifications unavoidable still for some time.

### C. Equation of State and Composition of Stellar Plasma

The nuclear and subnuclear EoS is an extremely important ingredient for SN modeling. Unfortunately, our knowledge of, in particular, the supranuclear regime is incomplete, although information from nuclear theory and experiment [123] as well as astrophysical observations, for example by the recently discovered  $1.97 M_\odot$  binary millisecond pulsar PSR J1614-2230 [124], is rapidly growing and is beginning to set serious constraints on the possible existence of bigger mass regions with exotic phases in NS interiors [125, 126].

The two EoSs for hot NS matter widely used for stellar core collapse in the past decade are those of Lattimer & Swesty [127] and Shen et al. [128]. They include nucleons and nuclei, electrons and positrons, and photons. The former is based on a compressible liquid-drop model [129] with a Skyrme force for nucleon interactions. The transition to homogeneous nuclear matter is established by a Maxwell construction. Most of the SN simulations by the Garching group were performed with a version (LS180-EoS) with an incompressibility modulus of bulk nuclear matter of  $K = 180$  MeV and a value of 29.3 MeV for the symmetry energy parameter. The Shen et al. EoS (STOS-EoS) employs a relativistic mean field model with parameter settings that reproduce characteristic properties of heavy nuclei. It is extended with the Thomas-Fermi spherical-cell approximation to describe homogeneous matter as well as inhomogeneous conditions. Its bulk incompressibility and symmetry energy have values of 281 MeV and 36.9 MeV, respectively.

These EoSs describe the nuclear composition as a mix of free nucleons, alpha particles, and a representative heavy nucleus, whose mass and charge numbers ( $A, Z$ ) depend on density, temperature, and neutronization of the matter. Although largely different ( $A, Z$ ) are returned by both EoSs during the infall stage and affect, for example neutrino trapping through coherent neutrino-nuclei scatterings, 1D simulations yield basically the same behavior. Quantitative differences occur only on a modest level of 5–25% in quantities characterizing collapse, bounce, and early postbounce evolution, e.g. in the central lepton fraction at neutrino trapping, position of shock formation, peak luminosity of the  $\nu_e$  burst, and maximum radius to which the shock expands before it retreats again [17, 130–132]. This outcome is even more astonishing in view of the appreciably different adiabatic index  $\Gamma = (\partial \ln P / \partial \ln \rho)_s$  ( $P$ ,  $\rho$ , and  $s$  are pressure, density, and entropy per nucleon, respectively) for both EoSs around nuclear density ( $\Gamma_{\text{LS}} \sim 2.2$ ,  $\Gamma_{\text{STOS}} \sim 2.9$ ) and the correspondingly different maximum compression and rebound behavior at bounce. Once again *Mazurek’s Law* applies, according to which any change of the microphysics is moderated in its effects on collapsing stellar cores by a

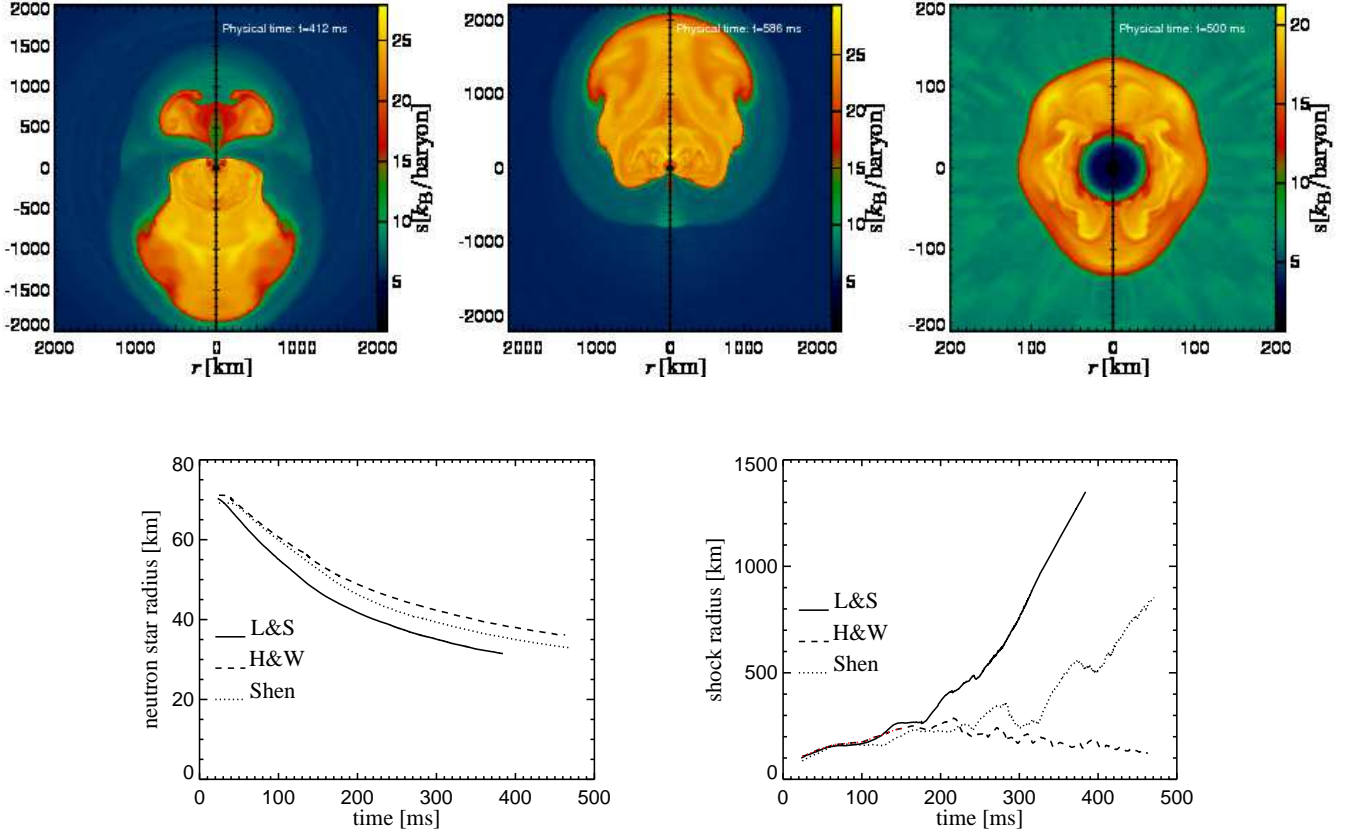


FIG. 4: Two-dimensional SN simulations [121] of an  $11.2 M_{\odot}$  star [22] for three different nuclear EoSs. The *upper panels* show cross-sectional entropy distributions at 412 ms after bounce for the LS180-EoS (*left*), at 586 ms p.b. for the STOS-EoS (*middle*), and at 500 ms p.b. for the Hillebrandt & Wolf EoS [122]. The last is the stiffest EoS of the set. It leads to the slowest contraction of the PNS (*bottom left*) and because of weaker neutrino heating and less vigorous hydrodynamic mass motions does not yield an explosion within the simulated time as visible in the evolution of the average shock radius (*bottom right*).

strong feedback between the EoS, weak interactions, neutrino transport, and hydrodynamics [133].

In order to achieve a more elaborate treatment of the nuclear composition in the shock-heated region below neutronospheric densities after bounce and to connect smoothly to the chemical abundances of the progenitor star, the Garching simulations employ at  $\rho < 10^{11} \text{ g/cm}^3$  a Boltzmann-gas NSE description with typically two dozen nuclear species, and in the non-NSE regime at  $T \lesssim 5 \times 10^9 \text{ K}$  a nuclear “flashing” treatment [91] or, alternatively available now, a small reaction network for nuclear burning.

With a maximum gravitational mass of  $1.83 M_{\odot}$  for cold NSs in weak equilibrium, the LS180-EoS is not compatible with PSR J1614-2230. Moreover, an incompressibility of  $K = 180 \text{ MeV}$  seems in conflict with the experimentally favored value of  $K \sim 240 \text{ MeV}$  for symmetric nuclear matter [134, 135]. While the STOS-EoS ( $M_{\text{max}}^{\text{STOS}} \approx 2.22 M_{\odot}$ ) fulfills both constraints, its radius of  $\sim 15 \text{ km}$  for a  $1.4 M_{\odot}$  NS does not match the best NS radius estimate from the currently most comprehensive evaluation of astrophysical data,  $R_{\text{ns}} \sim 11\text{--}12.5 \text{ km}$  for  $M_{\text{ns}} = 1.4 M_{\odot}$  [126]. This estimate overlaps with the range of  $\sim 10\text{--}14 \text{ km}$  deduced from theoretical considerations [123], which in turn agrees with a NS radius of  $\sim 12 \text{ km}$  for the LS180-EoS.

The properties of cold, neutronized NSs, however, are not necessarily conclusive for the conditions in the hot SN-core environment. Indeed, for different versions of the LS-EoS with  $K = 180, 220, 375 \text{ MeV}$  (the last two being compatible with PSR J1614-2230) the structure of hot PNSs well below the maximum mass, which is a relevant aspect for the early postbounce evolution of collapsing stellar cores, shows only smaller differences. Correspondingly, 1D CC simulations with these EoS versions revealed only minor differences until hundreds of ms after bounce [131, 136, 137]. During the later PNS cooling phase and in particular when mass accretion brings the PNS close to the mass limit, differences in the stiffness and the symmetry energy of the EoS can have important consequences, e.g. for the time when BH formation occurs [132] or for convective activity in the PNS and its influence on the neutrino emission [138]. Moreover, 2D simulations showed [106, 121] that the explosion of  $11.2 M_{\odot}$  and  $15 M_{\odot}$  progenitors depends sensitively on the radius evolution of the PNS in the first few 100 ms after bounce, i.e., the *radius contraction of the PNS* (in

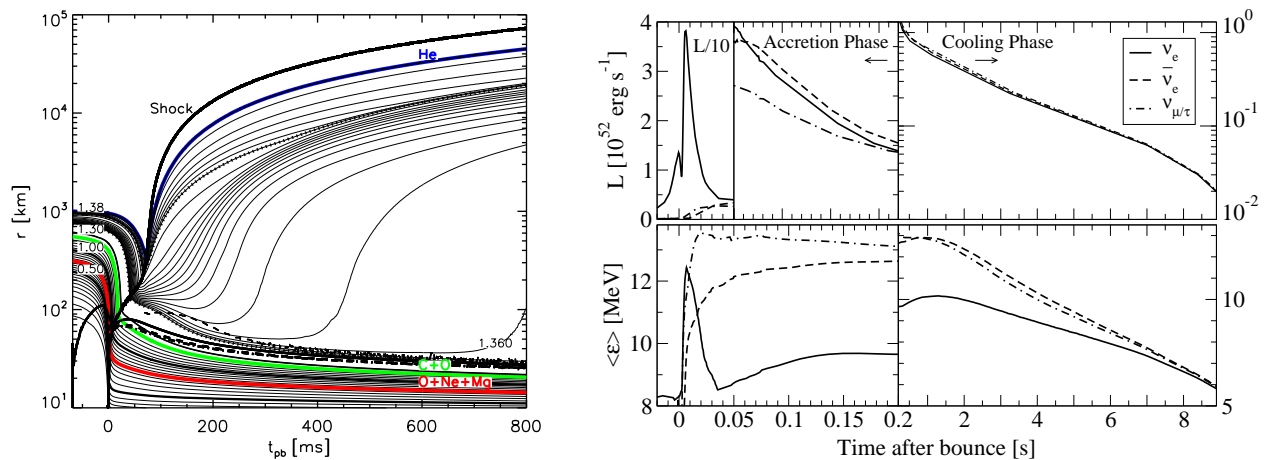


FIG. 5: *Left panel:* Neutrino-powered ECSN of an  $8.8 M_{\odot}$  star with ONeMg core [21, 28] visualized by mass-shell trajectories of a 1D simulation (from [105]). The SN shock (bold, outgoing line) expands for  $\sim 50$  ms as accretion shock (the downstream velocities are negative) before it accelerates by reaching the steep density gradient at the edge of the core. Neutrino heating subsequently drives a baryonic “wind” off the PNS surface. Colored lines mark the inner boundaries of the Mg-rich layer in the O-Ne-Mg core (red; at  $\sim 0.72 M_{\odot}$ ), C-O shell (green; at  $\sim 1.23 M_{\odot}$ ), and He-shell (blue; at  $\sim 1.38 M_{\odot}$ ). The outermost dashed line indicates the gain radius, and the inner (bold) solid, dashed, and dash-dotted lines are the neutrinospheres of  $\nu_e$ ,  $\bar{\nu}_e$ , and  $\nu_x$ , respectively. *Right panel:* Neutrino luminosities and mean energies from an ECSN for the infall,  $\nu_e$  breakout-burst, accretion phase, and PNS cooling evolution (from [107]). The average energies are defined as the ratio of energy to number fluxes. (The left panel is reproduced with permission; copyright: ESO.)

contrast to the final radius of the NS), because a more rapidly shrinking remnant radiates neutrinos with higher fluxes and energies [130, 132], thus enhancing neutrino heating and in particular also enabling more violent hydrodynamic instabilities (Fig. 4).

A variety of new non-zero temperature EoSs for SN studies have been put out recently [139–142]. With modern 1D SN codes being available, these EoSs have been (or will be) channelled through an “industrial” testing pipeline, confirming the modest influence of differences near or above nuclear-matter density on the early shock evolution in 1D as reported from previous studies above [132]. Also a refined description of the nuclear composition [132, 139] did not manifest itself in a big impact on infall and shock formation. Future studies, also in 2D and 3D, will have to show whether so far ignored light nuclei ( $^2\text{H}$ ,  $^3\text{H}$ ,  $^3\text{He}$ , Li) besides  $^4\text{He}$  [143–145] will have any relevant effects on the SN mechanism [132, 143] or the neutrino-driven wind from the cooling PNS [146].

#### IV. EXPLOSION MECHANISMS

In this section we will review the mechanisms by which the gravitational binding energy of the collapsing stellar core can be tapped to eject the outer stellar layers in a SN blast. A particular problem in understanding the onset of the explosion of massive stars is connected to the need of reversing implosion to explosion by transferring energy from the nascent NS to the overlying shells. This is different from thermonuclear SNe (SNe Ia) of white dwarfs (WDs), where the combustion (by deflagration or detonation) of carbon and oxygen to nickel and silicon in an essentially hydrostatic object releases sufficient energy to unbind and destroy the whole star.

The typical energy scale of the explosion of a WD near its Chandrasekhar mass limit is set by the release of nuclear binding energy associated with the conversion of  $\sim 1 M_{\odot}$  C+O to Si+Ni (roughly  $2 \times 10^{51}$  erg) minus the gravitational binding energy of the initial, highly degenerate WD (several  $10^{50}$  erg). But what sets the energy scale of CCSNe? Why does the large majority of “normal” cases have explosion energies similar to SNe Ia? The answer to this question is connected to the initial state of the dying star, in which the gravitationally unstable Fe-core is a configuration resembling a massive, degenerate WD, surrounded by dense shells whose gravitational binding energy is of the same order of magnitude, i.e., around  $(1\text{--}15) \times 10^{50}$  erg.

Any self-regulated mechanism for powering the explosion will deposit an energy in this range, possibly a few times this value, before the energy transfer is turned off. The neutrino-heating mechanism is such a self-regulated process, because the matter particles absorbing energy from neutrinos will react by expanding away from the heating region as soon as they have acquired an energy of the order of their binding energy. This will evacuate the heating region and diminish further energy input. But CC events show a large diversity concerning their kinetic energy, ranging

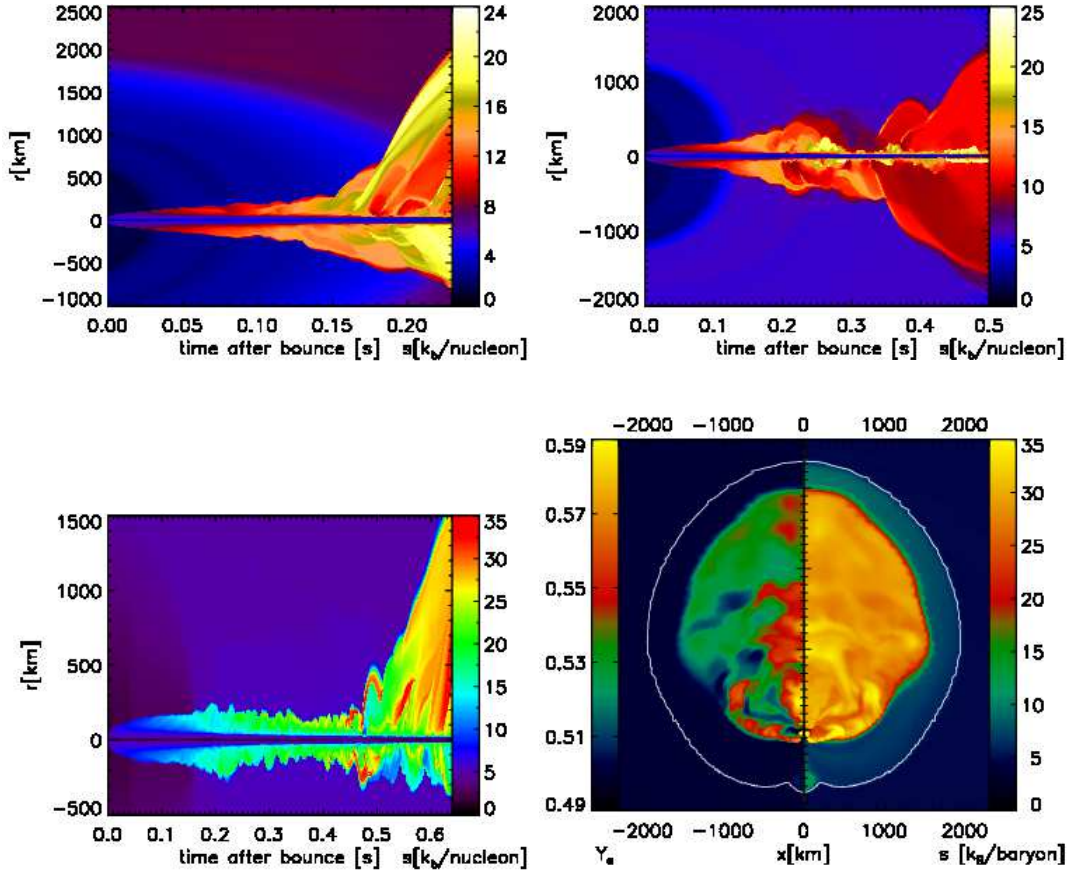


FIG. 6: Neutrino-driven explosions of Fe-core progenitors [81, 147]. The *upper left*, *upper right*, and *lower left* panels display the time evolution of color-coded entropy profiles in the north and south pole directions for 2D simulations of an  $8.1 M_{\odot}$  ultra metal-poor ( $10^{-4}$  solar metallicity) star (A. Heger, private communication), and  $11.2 M_{\odot}$  [22] and  $15 M_{\odot}$  [23] solar-metallicity stars, respectively. The shock position is clearly visible as a sharp boundary between high-entropy (yellow, red) and low-entropy (blue, black) regions. Shock oscillations are associated with violent convective activity in the neutrino-heating region and strong, bipolar SASI sloshing motions of the whole postshock layer. The explosions develop highly aspherically in all cases. The *lower right panel* shows, for example, an extreme dipole asymmetry of the cross-sectional distribution of electron fraction ( $Y_e$ ; *left*) and entropy at 775 ms p.b. for the  $15 M_{\odot}$  model, which explodes in a unipolar way. The NS is located at the position of the lowermost long tickmark on the vertical axis, far away from the geometrical center of the roundish shock contour (white line).

from  $\gtrsim 10^{50}$  erg to some  $10^{51}$  erg for SNe and up to several  $10^{52}$  erg for HNe (Fig. 3). Explosion energies far in excess of the initial gravitational binding energy of the ejecta suggest a different driving mechanism than neutrino heating, a process without the self-regulation described above. Magnetorotational explosions fulfill this requirement, because the blast-wave energy is extracted from the huge reservoir of rotational energy of a rapidly spinning PNS by magnetic fields and can be delivered in the form of electromagnetic energy.

In the following the status of our present understanding of both of these mechanisms will be summarized and also other, more controversial suggestions will be addressed.

### A. Thermonuclear Mechanism

While ignition of thermonuclear combustion in compression-heated, free-falling shells was recognized not to be able to blow matter outwards [6], Russian authors [148–151] later proposed neutrino radiation from the collapsing stellar core to heat the degenerate C+O shell of a low-mass progenitor star at hydrostatic conditions and a density around  $2 \times 10^9 \text{ g/cm}^3$  and thus to ignite a thermonuclear burning front that explodes the star. The heating was considered to be mainly by neutrino-electron scattering.

Although this is a cute idea, neither the stellar nor the dynamical conditions assumed for this scenario could be

verified by detailed progenitor and explosion models. In ONeMg-core progenitors, for example, which define the low-mass limit of stars that undergo core collapse to radiate large neutrino luminosities, the C+O shell is initially located between roughly 500 and 1000 km (at densities  $\lesssim 4 \times 10^8 \text{ g/cm}^3$ ) and falls dynamically inward (with compression-induced burning) much before it is exposed to a high fluence of neutrinos (see Fig. 5). If, in contrast, the O and C layers are farther out at  $r > 1000 \text{ km}$  as in more massive Fe-core progenitors (Fig. 2), the neutrino flux is diluted by the large distance from the source and the electron densities (and degeneracy) there are much lower than adopted in [148–151] so that neutrino-electron scattering cannot raise the temperature to the ignition threshold.

Presently PISNe are the only stellar CC events where the explosion mechanism is known to be based on thermonuclear energy release (Sect. IID), but a closer examination of the possibility of neutrino-triggered burning in the significantly more compact low-metallicity stars might be interesting.

## B. Bounce-Shock Mechanism

The purely hydrodynamical bounce-shock mechanism [4, 5], in which the shock wave launched at the moment of core bounce (Sect. IIB) causes the “prompt” ejection of stellar mantle and envelope, has been a matter of intense research in the 1980’s (for a review, see [152]). However, for more than 20 years now detailed analytical analysis of collapse and bounce physics (e.g., [153] and refs. therein) as well as all modern CC simulations—despite continuous improvements and significant quantitative differences in details, mainly linked to important refinements of electron captures on heavy nuclei and neutrino-electron scattering during infall—agree in the basic outcome: The prompt mechanism cannot succeed in causing the explosion of any progenitor star.

Upgrades of the microphysics turned out to disfavor prompt explosions by decreasing the size of the homologously and subsonically collapsing “inner core”, whose mass scales with the instantaneous Chandrasekhar mass,  $M_{\text{Ch}}(t) \propto Y_e^2(t)$ , and whose edge defines the location of shock formation at bounce. (The number fraction  $Y_i$  of particles, here of electrons ( $e$ ), is defined as the number of particles ( $i$ ) per nucleon.) With the presently most sophisticated treatment of neutrino emission by electron captures on nuclei and free protons during core infall [55] the central electron fraction  $Y_{e,c}$  after neutrino trapping decreases to 0.25–0.27 (corresponding to a trapped lepton fraction of 0.285–0.30), and the shock formation point (defined by the location where the entropy first reaches a value of  $3 k_B$  per nucleon) lies at an enclosed mass of only  $0.4\text{--}0.5 M_\odot$  [17, 104, 154]. Moreover, because preferred nuclear EoSs are relatively stiff, the rebound of the inner core is too weak to transfer a large energy to the shock. The flow discontinuity, running into supersonically infalling material at densities below  $\sim 10^{13} \text{ g/cm}^3$ , quickly loses its initial energy by heating the plasma to entropies of several  $k_B$  per nucleon and thus disintegrating heavy nuclei to free nucleons (which consumes roughly  $1.7 \times 10^{51} \text{ erg}$  per  $0.1 M_\odot$ ). A short transient period of positive postshock velocities therefore lasts only 1–2 ms, after which the velocity in the whole postshock region becomes negative again. A negative postshock velocity defines the moment of shock stagnation, at which time the shock has travelled through just  $0.3\text{--}0.35 M_\odot$  of iron material and is still deep inside the stellar Fe-core. Since the preshock density then is still above  $10^{11} \text{ g/cm}^3$ , shock stagnation happens well before shock breakout and thus before the release of the prompt burst of  $\nu_e$ . Lepton number and energy ( $\sim 2 \times 10^{51} \text{ erg}$ ) drain by the escape of the  $\nu_e$  burst is therefore not causal for the shock stagnation.

Despite negative velocities and thus accretion flow to the central NS in the downstream region of the shock, the latter continues to propagate outward in mass as well as radius. This motion of the shock stagnation radius is a response to the massive accretion of infalling matter (initially with a rate  $\dot{M} \gg 1 M_\odot/\text{s}$ ; cf. Fig. 5), which emits energy and lepton number in neutrinos and thus settles onto the PNS only gradually, creating the postshock pressure that pushes the shock position outwards. Finally, after reaching a maximum radius of typically 100–150 km, the accretion shock retreats again in 1D models, following the contraction of the nascent NS roughly according to the relation

$$R_s \propto \frac{(L_\nu \langle \epsilon_\nu^2 \rangle)^{4/9} R_{\text{ns}}^{16/9}}{\dot{M}^{2/3} M_{\text{ns}}^{1/3}} \propto \frac{R_{\text{ns}}^{8/3} (k_B T_\nu)^{8/3}}{\dot{M}^{2/3} M_{\text{ns}}^{1/3}} \propto \frac{L_\nu^{4/3}}{\dot{M}^{2/3} M_{\text{ns}}^{1/3} (k_B T_\nu)^{8/3}}, \quad (2)$$

which can be derived by combining equations (33, 39, 43, 44, 56, 63) of ref. [155] and assuming  $R_g \propto R_{\text{ns}}$  for the “gain radius”  $R_g$  (see Sect. IV C) as well as  $L_\nu \propto R_{\text{ns}}^2 T_\nu^4$ , and  $\langle \epsilon_\nu^2 \rangle \propto (k_B T_\nu)^2$  for neutrino ( $\nu \in \{\nu_e, \bar{\nu}_e\}$ ) luminosity and mean squared energy, respectively. The radius of maximum shock expansion at this stage is still well below the dissociation radius of iron, for which the equality  $GM_{\text{ns}} m_u / R_{\text{diss}} = 8.8 \text{ MeV}$  ( $m_u$  is the atomic mass unit) yields  $R_{\text{diss}} \approx 200 \text{ km}$ . This means that the matter behind the shock is fully disintegrated into neutrons and protons.

It is during this period of  $\sim 100 \text{ ms}$  of slow shock expansion that a “gain radius” emerges, at which energy losses by neutrinos for  $r < R_g$  change to neutrino heating for  $r > R_g$  [7]. Before this moment neutrino losses are dominant in the whole postshock layer. The onset of neutrino-energy deposition also allows convective activity to develop behind the shock: Neutrino heating creates a negative entropy gradient  $ds/dr$ , which is unstable in the strong gravitational

field according to the Ledoux criterion,

$$C_L = \left( \frac{\partial \rho}{\partial s} \right)_{Y_e, P} \frac{ds}{dr} + \left( \frac{\partial \rho}{\partial Y_e} \right)_{s, P} \frac{dY_e}{dr} > 0. \quad (3)$$

This criterion, however, defines growth conditions for convection and Rayleigh-Taylor structures exactly only for a static layer, but needs to be generalized for the infalling flow in the postshock region [76, 104, 156]. Convective activity can take place there only when the inward advection timescale  $t_{\text{adv}} \sim r/|v_r|$  for radial velocity  $v_r$  is sufficiently longer than the convective growth timescale of perturbations (inverse Brunt-Väisälä or buoyancy frequency),  $t_{\text{conv}} \sim (g_{\text{grav}}|C_L|/\rho)^{-1/2}$ , or than the buoyancy acceleration timescale,  $t_{\text{buoy}} \sim (g_{\text{grav}}(\delta\rho/\rho)/r)^{-1/2}$ , of blobs with density contrast  $\delta\rho/\rho$  in a local gravitational field with acceleration  $g_{\text{grav}} = GM/r^2$  [156, 157].

The breaking of spherical symmetry by hydrodynamic instability, manifesting itself in the growth of initially small, random seed perturbations to large-scale structures, turned out to be generic to the shock stagnation phase in collapsing stellar cores and to be decisive for the success of the neutrino-heating mechanism and for the further destiny of the stalled accretion shock.

### C. Neutrino-Heating Mechanism

The development of a neutrino-heating layer is a natural consequence of the contraction of the PNS and associated compactification of its surrounding accretion layer during the postbounce accretion phase. The contraction of the PNS leads to increasing neutrinospheric temperatures and therefore growing mean energies of the radiated neutrinos (Fig. 7). More energetic neutrino emission together with the decreasing postshock temperature at larger shock radii allows for the appearance of a gain radius: Since the temperature in the postshock layer drops roughly like  $r^{-1}$  (this is well fulfilled for convectively mixed, isentropic conditions, while in 1D the gradient is even steeper), the neutrino-cooling rate per nucleon by captures of (nondegenerate)  $e^-$  and  $e^+$  on protons and neutrons drops with  $q_\nu^- \propto T^6 \propto r^{-6}$ . In contrast, the neutrino-heating rate per nucleon (which is largely dominated by  $\nu_e, \bar{\nu}_e$  absorption on free  $n, p$ , respectively) scales with  $q_\nu^+ \propto L_\nu \langle \epsilon_\nu^2 \rangle r^{-2}$  and thus decreases less steeply with  $r$  than  $q_\nu^-$ , enabling a crossing point  $R_g$  to occur [7], where  $T_g^3 R_g \propto \sqrt{L_\nu \langle \epsilon_\nu^2 \rangle}$ .

#### 1. Heating Efficiency and Energetics

With a density profile  $\rho \propto r^{-3}$  between gain radius  $R_g$  and shock  $R_s$  (see, e.g., [155]) and the preshock (free-fall) velocity  $v_0 = -\sqrt{2GM_{\text{ns}}/R_s}$ , mass infall rate  $\dot{M} = 4\pi R_s^2 |v_0| \rho_0$  of the progenitor star, and density jump at the shock,  $\beta = \rho_1/\rho_0 \sim 10$ , the optical depth for  $\nu_e$  and  $\bar{\nu}_e$  absorption in the gain layer can be estimated as

$$\tau \approx 0.026 \left( \frac{k_B T_\nu}{4 \text{ MeV}} \right)^2 \left( \frac{\dot{M}}{0.1 M_\odot \text{ s}^{-1}} \right) \left( \frac{R_s}{200 \text{ km}} \right)^{3/2} \left( \frac{R_g}{100 \text{ km}} \right)^{-2} \left( \frac{M_{\text{ns}}}{1.5 M_\odot} \right)^{-1/2}, \quad (4)$$

where  $Y_n \approx Y_p \approx 0.5$  and  $\langle \sigma_{\text{abs}} \rangle \approx 3.26 \times 10^{-41} [k_B T_\nu / (4 \text{ MeV})]^2 \text{ cm}^2$  for the average absorption cross section of a blackbody neutrino spectrum with temperature  $T_\nu$  (therefore  $\langle \epsilon_\nu^2 \rangle \approx 21 (k_B T_\nu)^2$ ) was used. Equation 4 suggests that for typical accretion rates,  $\dot{M} = 0.1\text{--}0.5 M_\odot/\text{s}$ , several percent of the neutrino luminosity from the neutrinosphere can be absorbed in the gain layer, thus accounting for a neutrino-heating rate  $Q_\nu^+ = \tau (L_{\nu_e} + L_{\bar{\nu}_e}) \approx 10^{51}\text{--}10^{52} \text{ erg/s}$  for  $\nu_e$  and  $\bar{\nu}_e$  luminosities,  $L_\nu$ , of some  $10^{52} \text{ erg/s}$  during the postbounce accretion phase (Fig. 7).

However, in a dynamical situation as in the gain layer, where the matter is not at rest, the optical depth (which determines the interaction probability of a crossing neutrino) is not a perfectly appropriate measure for the heating efficiency. This holds in particular in the multi-dimensional case, where accretion funnels carry cold (low-entropy) matter from the shock towards the NS, while neutrino-heated matter expands outward in high-entropy bubbles. At such conditions the residence time of the matter in the gain layer accounts for the duration of its exposure to neutrino heating. While in the 1D case the advection time  $t_{\text{adv}} \sim (R_s - R_g)/|v_1|$  with  $v_1 = v_0/\beta$  measures how long the accretion flow needs from  $R_s$  to  $R_g$  [157, 158], the dwell time in the gain region is better captured in the multi-D situation by the more general expression [104, 106]

$$t_{\text{dwell}} \approx \frac{M_g}{\dot{M}}, \quad (5)$$

which relates the mass in the gain layer  $M_g$  with the mass accretion rate  $\dot{M}$  through the shock and (for conditions near steady state) through the gain radius. With an energy-transfer rate per nucleon by neutrino absorption of



$q_\nu^+ = n_\nu \langle \epsilon_\nu \rangle \langle \sigma_{\text{abs}} \rangle c$ , where  $n_\nu \langle \epsilon_\nu \rangle = L_\nu / (4\pi r^2 c)$ , each nucleon absorbs an energy of  $q_\nu^+ t_{\text{dwell}} \sim 50 \text{ MeV}$  for time  $t_{\text{dwell}} \sim 0.1 \text{ s}$  when  $k_B T_\nu = 4 \text{ MeV}$ ,  $L_\nu = 3 \times 10^{52} \text{ erg/s}$  ( $\nu \in \{\nu_e, \bar{\nu}_e\}$ ), and  $r = R_g \sim 100 \text{ km}$  are assumed. This corresponds to a temperature of  $\sim 3 \text{ MeV}$  and an entropy of  $\sim 20 k_B$  per nucleon of an  $e^\pm$ -photon-dominated plasma at  $\rho \sim 10^9 \text{ g/cm}^3$  (cf. Figs. 4 and 6). The total energy deposition rate by  $\nu_e$  plus  $\bar{\nu}_e$  absorption in the gain layer thus becomes

$$Q_\nu^+ = q_\nu^+ \frac{M_g}{m_u} \sim 9.4 \times 10^{51} \frac{\text{erg}}{\text{s}} \left( \frac{k_B T_\nu}{4 \text{ MeV}} \right)^2 \left( \frac{L_\nu}{3 \cdot 10^{52} \text{ erg/s}} \right) \left( \frac{M_g}{0.01 M_\odot} \right) \left( \frac{R_g}{100 \text{ km}} \right)^{-2}. \quad (6)$$

Equation (6) corresponds to a heating efficiency of

$$\frac{Q_\nu^+}{L_{\nu_e} + L_{\bar{\nu}_e}} \sim 0.16 \left( \frac{k_B T_\nu}{4 \text{ MeV}} \right)^2 \left( \frac{M_g}{0.01 M_\odot} \right) \left( \frac{R_g}{100 \text{ km}} \right)^{-2} \quad (7)$$

and an integral energy deposition of

$$E_N \sim Q_\nu^+ t_{\text{dwell}} \sim 9.4 \times 10^{50} \text{ erg} \left( \frac{k_B T_\nu}{4 \text{ MeV}} \right)^2 \left( \frac{L_\nu}{3 \cdot 10^{52} \text{ erg/s}} \right) \times \left( \frac{M_g}{0.01 M_\odot} \right)^2 \left( \frac{\dot{M}}{0.1 M_\odot \text{ s}^{-1}} \right)^{-1} \left( \frac{R_g}{100 \text{ km}} \right)^{-2}. \quad (8)$$

These numbers, reduced by 20–30% for neutrino-cooling losses in the gain layer, are well compatible with results of detailed simulations [81, 106].

## 2. Hydrodynamical Explosion Models

Neutrino-driven explosions can be found in 1D simulations only for ECSNe of low-mass progenitors ([105, 159, 160], considering an  $8.8 M_\odot$  star with an ONeMg core [21, 28]). Because of the extremely steep density gradient at the edge of the ONeMg core and the corresponding rapid decrease of  $\dot{M}$ , the radius of the accretion shock grows continuously (cf. Eq. 2), thus creating ideal conditions for neutrino-energy transfer (Fig. 5). The latter drives a baryonic outflow, which carries the energy for the explosion. With the most sophisticated available treatment of neutrino-matter interactions (Table I; Sect. III B) an explosion energy  $E_{\text{ONeMg}} \approx 10^{50} \text{ erg}$  was obtained [105, 159], which is enhanced at most by  $\sim 10\%$  in 2D models due to a brief phase ( $\sim 50$ – $200 \text{ ms}$  p.b.) of convective overturn behind the rapidly expanding shock [33, 159]. The low explosion energy and little nickel ejection (several  $10^{-3} M_\odot$ ; [33]) are compatible with estimates for the Crab SN ([34] and refs. therein).

For more massive Fe-core progenitors nonradial hydrodynamic instabilities —convective overturn [8, 9, 11, 73] in combination with SASI activity [84]— turned out to be decisive for the success of the neutrino-heating mechanism [104, 106]. While 1D models did not explode, the Garching group found neutrino-driven, though weak, explosions for  $11.2$  and  $15 M_\odot$  stars in 2D simulations [104, 106]. Recently, these results with the Prometheus-VERTEX program [80, 91] could be confirmed by general relativistic 2D simulations [81] based on the newly developed CoCoNut-VERTEX code [103], which also produced explosions for solar-metallicity  $27 M_\odot$  and metal-poor ( $10^{-4}$  solar metallicity)  $8.1 M_\odot$  progenitors with Fe cores (see Fig. 6 and [161]).

Neutrino-driven explosions for a variety of stars were also seen in 2D and 3D simulations of other groups with different multi-group treatments of neutrino transport [97–99, 116], whereas the Arizona-Jerusalem-Princeton (AJP) collaboration could not observe any success of the neutrino-heating mechanism [108, 109]. This underlines the sensitivity of the outcome qualitatively and quantitatively to details of the input and methods. While there are many differences between the modeling approaches concerning numerics and microphysics, the Garching 2D models in particular include the full set of neutrino-matter interactions of Table I and a careful implementation of all fluid-motion dependent terms as well as GR effects in the transport. All were recognized to be significant [79, 80] but were simplified or ignored in the AJP calculations due to the omission of energy-bin coupling there (see also Sect. III B). Instead of attributing conflicting results to transport differences, it has been repeatedly stated that the success of the Garching simulations is disputable because the unacceptably soft LS180-EoS was used (e.g., [162]). This criticism, however, misses foundation because of the arguments given in Sect. III C and the fact that the  $11.2 M_\odot$  explosion could be

reproduced with the stiffer STOS-EoS (Fig. 4), which did not lead to an explosion in the  $11.2 M_\odot$  run of the AJP collaboration [109].

Self-induced neutrino-flavor conversions in the SN core, which could swap lower-energetic  $\nu_e$  and  $\bar{\nu}_e$  spectra with hotter  $\nu_x$  and  $\bar{\nu}_x$  spectra and thus might enhance the neutrino heating behind the shock and strengthen the SN explosion, have recently been shown not to have an impact during the postbounce accretion phase. Because detailed SN models yield electron densities that are higher than the neutrino densities (mostly even  $n_e \gg n_\nu$ ), the matter background dominates and thus suppresses collective neutrino oscillations by dephasing the flavor evolution of neutrinos travelling on different trajectories [163–166].

### 3. Effects of Nonspherical Flows

Nonradial, turbulent flows increase the residence time of matter in the gain layer [98, 104, 167] and thus the mass  $M_g$  in this region (for given  $\dot{M}$ ; Eq. 5). This leads to a higher total energy deposition rate by neutrinos,  $Q_\nu^+$  (Eq. 6), and to an enhanced integral energy transfer  $E_N$  (Eq. 8).

Rayleigh-Taylor fingers, for example, which develop in a convectively unstable situation (Eq. 3) channel cool, freshly accreted material from immediately downstream of the shock towards the PNS and thus closer to the gain radius, where neutrino heating is strongest. At the same time, expanding bubbles of buoyant, high-entropy gas allow freshly heated matter to rise away from the gain radius instead of being accreted inward to the cooling layer. This reduces energy losses by the reemission of neutrinos, which can have important dynamical consequences because cooling for  $r < R_g$  is usually much larger than net heating in the gain layer. The combination of all such effects leads to an increase of the temperature and pressure in the gain layer, which in turn pushes the shock farther out. A positive feedback cycle is the consequence, which for sufficiently strong neutrino heating enables an explosion in the multi-D case even when the neutrino-driven mechanism fails in 1D.

SASI activity can basically have the similar effects. It is not only associated with shock expansion and nonradial mass flows, thus allowing for a larger efficiency of neutrino-energy deposition, it also leads to secondary shocks that dissipate kinetic energy and produce extra heating and higher entropies, strengthening the convective activity and giving additional push to the shock [76, 106].

After the onset of the explosion, the nonspherical situation permits simultaneous shock expansion and ongoing accretion. This maintains higher neutrino fluxes and stronger neutrino heating for a longer time compared to the 1D case [106], where the accretion luminosity decays as soon as shock expansion quenches the mass infall to the PNS.

While hydrodynamical simulations clearly demonstrate that violent convective and SASI activity are crucial for the success of the neutrino-heating mechanism [161], the nature of the SASI and the exact role of hydrodynamic instabilities and turbulent motions for the onset of the explosion are still a matter of intense research. The SASI, whose amplitude grows from small pressure and/or entropy perturbations in an oscillatory way with highest growth rates for the lowest-order spherical harmonics (dipolar  $\ell = 1$  and quadrupolar  $\ell = 2$ ) components [84, 168–170], seems to be an ideal candidate to explain not only the global asymmetries found in the SN core in simulations, but also the large asphericities and mixing effects that are observed in most SNe and SN remnants and that are probably linked to the measured high kick velocities of many young pulsars (cf. Sect. VI). Linear growth analysis, numerical toy models for the linear and nonlinear regimes [76, 171], and laboratory shallow-water experiments [172] yield evidence that the underlying instability mechanism is an advective-acoustic cycle [173, 174] rather than a purely acoustic one [168].

### 4. Runaway Threshold

Burrows & Goshy [175] conjectured the transition to the explosion to be a global instability of the postshock layer. Considering steady-state accretion conditions in 1D, they determined a critical neutrino luminosity  $L_{\nu,c}(\dot{M})$  as a function of the mass accretion rate that damps shock expansion (cf. Eq. 2), above which they could not find accretion solutions and thus expected the onset of the explosion. Their reasoning is supported by subsequent similar analyses of stationary accretion flows [176–178] as well as hydrodynamical studies [11, 87, 88, 167, 179].

The existence of a functional relation  $L_{\nu,c}(\dot{M})$  as threshold condition to an explosion can be qualitatively understood by simple analytic considerations. Numerical simulations [104, 106, 167, 179, 180] have shown that the necessary condition for runaway expansion is given by  $t_{\text{adv}}/t_{\text{heat}} > 1$ , i.e., the explosion can set in when the advection timescale of the mass flow through the gain layer,

$$t_{\text{adv}} = \int_{R_g}^{R_s} \frac{dr}{|v_r|} \sim \beta \frac{R_s}{|v_0|} \sim \beta \frac{R_s^{3/2}}{\sqrt{2GM_{\text{ns}}}}, \quad (9)$$



exceeds the heating timescale for neutrinos to deposit enough energy to lift matter from a gravitationally bound to an unbound state. In this context the total energy of the gas is the relevant quantity, i.e., the sum of internal, gravitational, and kinetic energies, which in a bound state is negative. Making the assumption that this energy scales roughly with the gravitational energy near the gain radius, which for a nucleon is  $\epsilon_g = -GM_{\text{ns}}m_u/R_g$ , one obtains

$$t_{\text{heat}} \sim \frac{|\epsilon_g|}{q_\nu^+} \propto \frac{M_{\text{ns}}R_g}{L_\nu \langle \epsilon_\nu^2 \rangle}. \quad (10)$$

Setting both timescales equal,  $t_{\text{adv}} = t_{\text{heat}}$ , and using Eq. (2) for  $R_s$  and the fact that  $R_g$  follows approximately  $R_{\text{ns}}$ , i.e.,  $R_g \propto R_{\text{ns}} \propto L_\nu^{1/2}/(k_B T_\nu)^2$  (which was also applied in deriving Eq. 2), leads to

$$L_{\nu,c}(\dot{M}) \propto \beta^{-2/5} \dot{M}^{2/5} M_{\text{ns}}^{4/5}. \quad (11)$$

This relation reproduces the functional behavior found in [175] very well (the numerical factor of the scaling relation becomes  $(5\text{--}6) \times 10^{52} \text{ erg/s}$  for  $\beta \sim 10$ ,  $\dot{M} = 1 M_\odot/\text{s}$ , and  $M_{\text{ns}} = 1.5 M_\odot$ , slightly varying with the choice of other involved parameters). It must be pointed out, however, that the limiting luminosity for steady-state accretion solutions as derived in [175] was shown to be usually close to, but not identical with the runaway threshold at  $t_{\text{adv}} > t_{\text{heat}}$ . The latter roughly coincides with the time when the fluid behind the shock begins to develop positive total specific energy (see the excellent study of [179]).

Numerous studies for both stationary accretion flows [176, 177] and time-dependent conditions in collapsing stellar cores [11, 87, 88, 167] have demonstrated that the critical neutrino luminosity for fixed mass accretion rate is significantly lowered in the multi-dimensional case, typically by several 10%. The possible (or combined) reasons for this improvement were discussed in Sect. IV C 3, but many aspects are still unsettled. For example, the properties and consequences of neutrino-driven turbulence (e.g., convective energy transport and pressure) are a matter of ongoing research [181] and the effects of 3D hydrodynamics have not been clarified yet. While there is hope that these might make the runaway easier than in 2D [87, 98] and thus lead to earlier and more powerful explosions, not all studies revealed a significant reduction of the threshold luminosity in 3D relative to 2D [88]. The 2D/3D comparison obviously depends on subtle differences of the background flow, neutrino source terms or even numerics, and requires further exploration. A sophisticated neutrino transport seems necessary for reliable answers.

### 5. Modes of Global Instability

The results of SN simulations and analytic studies suggest that the onset of the explosion is connected to a global runaway instability of the postshock accretion layer [130, 175] fueled by neutrino energy deposition above a certain threshold (see Sect. IV C 4). An important question concerns the type of mode that grows fastest to trigger the runaway [179]. Unstable oscillatory and non-adiabatic radial modes were observed in many time-dependent 1D simulations—in agreement with linear stability analysis [182]—for neutrino luminosities intermediate between those that are too low to drive explosions and those that suffice to trigger an explosion by the instability of a nonoscillatory radial mode [11, 80, 87, 88, 167, 169, 179, 183]. But what happens in the multi-dimensional case? Is the runaway there caused by an unstable radial oscillatory or nonoscillatory mode, whose development is affected by turbulence altering the conditions of the background flow? Or is a nonradial nonoscillatory (possibly convective) or oscillatory (SASI) mode decisive? Exploration of the growth conditions has only begun, suggesting that unstable large-scale, nonoscillatory modes require the highest driving luminosities [182], but their growth may strongly depend on the conditions in the SN core [161], the dimensionality of the problem, and even a modest rate of rotation [184]. While first 3D simulations [85, 87, 88, 95, 98, 99] show strongly damped or no radial oscillations, suggesting that SASI modes are less strong in 3D and the explosion might be connected to unstable nonoscillatory modes [185, 186], none of these simulations was performed with a combination of sufficiently sophisticated neutrino transport, high enough numerical resolution, and a consistent inclusion of all dissipative processes (such as the decay of the NS core luminosity, changes of the accretion luminosity, and the shrinking of the nascent NS, all of which provide a negative feedback) included and combined consistently. Final answers will require well-resolved, full-scale 3D radiation-hydrodynamics simulations with reliable neutrino treatment.

### D. Magnetohydrodynamic Mechanisms

MHD phenomena, in particular the magnetorotational mechanism (MRM) proposed in [187, 188], have been discussed as potential drivers of SN explosions already in the 1970's (e.g., [189, 190]) and were explored by first axisymmetric simulations with approximate microphysics and artificially imposed stellar core rotation and magnetic field

configurations in [65, 67]. These and a flood of subsequent 2D calculations, which either ignored or radically simplified the neutrino physics (e.g., [191–194] and refs. therein), or more recently used neutrino transport by MGFLD (assuming, inappropriately, the stellar medium to be at rest; [109]), have confirmed that MHD processes and especially the MRM are able viable agents to extract energy from a highly magnetized NS and to violently expel the outer stellar layers.

Because of the extremely low resistivity of SN matter, magnetic field lines are frozen in the flow. Magnetic flux conservation therefore leads to compressional amplification of the average strength of the nonradial field during CC,  $B \propto R_{\text{core}}^{-2} \propto \rho_{\text{core}}^{2/3}$ , and a corresponding growth of the energy density of the magnetic fields ( $\propto B^2$ ). Initial fields as expected in stellar cores at the onset of gravitational instability, i.e., several  $10^9$  G for the dominant toroidal component [36], can thus grow by a factor  $>1000$  but cannot gain dynamically relevant strength, for which the magnetic pressure has to reach a fair fraction of the gas pressure.

Therefore secondary amplification mechanisms are crucial to further boost the magnetic energy density to values close to equipartition with the stellar plasma. In the MRM such an increase in energy density can be achieved by tapping the huge reservoir of rotational energy,  $E_{\text{rot}} \propto J_{\text{core}}^2 / (M_{\text{core}} R_{\text{core}}^2)$ , that builds up at the expense of gravitational energy due to angular momentum ( $J_{\text{core}}$ ) conservation during the infall. The rotational energy in a rapidly spinning PNS with average revolution period  $P_{\text{ns}}$  thus becomes

$$E_{\text{rot}} \sim 2.4 \times 10^{52} \text{ erg} \left( \frac{M_{\text{ns}}}{1.5 M_{\odot}} \right) \left( \frac{R_{\text{ns}}}{10 \text{ km}} \right)^2 \left( \frac{1 \text{ ms}}{P_{\text{ns}}} \right)^2. \quad (12)$$

The amplification can either happen through the wrapping of an (initially present or convectively created) poloidal field, stretching it into a toroidal one, which leads to a linear increase with the number of windings. Or it can take place by exponential amplification with characteristic timescale of order  $4\pi |d\Omega/d \ln r|^{-1}$  (with  $\Omega(r) = 2\pi/P_{\text{rot}}(r)$ ) being the angular frequency for local spin period  $P_{\text{rot}}$ ) through the magnetorotational instability (MRI; [195, 196]), whose growth conditions in SN cores were studied in detail in [197]. Both processes require differential rotation, which naturally develops during infall. Saturation fields of order

$$B^2 \sim 4\pi \rho r^2 \Omega^2 \left( \frac{d \ln \Omega}{d \ln r} \right)^2 \quad (13)$$

can be expected in an MRI-unstable environment, in which  $d\Omega/d \ln r < 0$  must hold to enable the growth of long-wavelength, slow-magnetosonic waves. For sufficiently large angular velocities, fields of order  $10^{15}$ – $10^{16}$  G were estimated [196].

The ejection of matter can be driven by magnetic pressure and hoop stresses, magnetic buoyancy, or gas heating due to the dissipation of rotational energy through turbulent magnetic viscosity [180, 189, 196]. Well collimated, bipolar outflows or jets along the rotation axis with characteristic power

$$\dot{E}_{\text{MHD}} \sim 10^{52} \frac{\text{erg}}{\text{s}} \left( \frac{B}{10^{15} \text{ G}} \right)^2 \left( \frac{r}{30 \text{ km}} \right)^3 \left( \frac{\Omega}{10^3 \text{ rad s}^{-1}} \right) \quad (14)$$

may be generic [110, 196, 198].

Since the MRM can tap only the free energy of differential rotation in the PNS,  $E_{\text{rot}}^{\text{free}} \ll E_{\text{rot}}$ , angular velocities near the Keplerian rate of the progenitor core ( $P_{\text{core}} \sim 1$  s) are required for magnetic fields to grow to dynamical significance. SN simulations [110, 180] suggest that the spin period must be  $P_{\text{core}} \lesssim 2$ – $5$  s, leading to NSs rotation periods of  $P_{\text{ns}} \sim (R_{\text{ns}}/R_{\text{core}})^2 P_{\text{core}}$  under the assumption of strict angular momentum conservation. Present stellar evolution models that include angular momentum loss through magnetic breaking, however, yield typical core-rotation periods of  $P_{\text{core}} \gtrsim 100$  s before collapse (cf. Sect. II B). Such slowly rotating stellar cores are consistent with observed spin rates of newly born white dwarfs [199] and with the estimated spin periods of new-born pulsars of  $\sim 10$  ms [36, 200], but they are much too slow to provide the rotational energy reservoir for powering SNe through the MRM (see Eq. 12).

A variety of mechanisms have also been proposed for magnetic field amplification in collapsing cores with no or slow rotation, e.g. by a convective dynamo [201], turbulent SASI motions in the postshock region [202] or exponential steepening of Alfvén waves created by fluid perturbations at Alfvén points in the accretion flow of the PNS [203]. Moreover, Alfvén waves emitted from the convective layer inside the PNS (thus extracting energy from the rich reservoir of gravitational binding energy of the contracting remnant) were suggested to provide extra energy to the stalled SN shock by dissipative heating [204] similar to the heating of the solar corona by Alfvén waves emerging from the surface of the Sun. Recent 2D CC simulations with neutrino transport [114], however, find that these mechanisms are either inefficient or able to amplify the fields only locally. Large-scale fields with dynamical importance must reach magnetar strength (at least  $10^{14}$ – $10^{15}$  G) but in the absence of magnetorotational processes seem to require pre-collapse fields 100 times stronger than predicted by stellar evolution models.

Magnetic fields are therefore likely to play some role in all SN cores, but at the moment it seems only certain that they are crucial for the explosion of very rapidly spinning stars, which are probably linked to long GRBs and HNe (Sect. II C). MHD mechanisms have the advantage of not being strongly coupled to the mass in the gain layer and the mass-accretion rate through the stalled shock, which determine the explosion energy of SNe powered by neutrino heating (Eq. 8). MHD-driven explosions can therefore be considerably more energetic than neutrino-driven SNe, where blast-wave energies of  $\sim(1-2)\times 10^{51}$  erg may be the upper limit (see Sect. VI C). Large global deformation and well collimated jets must be expected to be generic to MHD explosions of very rapidly rotating stellar cores and seem to be characteristic of most hyperenergetic SNe Ib/c.

Reliable and predictive multi-dimensional simulations of such phenomena are hampered by the fact that the true nature of MHD phenomena can only be treated in 3D, and such models should also include reasonably realistic neutrino transport. Another problem arises from the extreme dependence of the dynamical evolution on the initial conditions, in particular the rotation rate and profile of the stellar core (e.g., [191–193]) and the initial strength and geometry of the magnetic field (e.g., [194] and refs. therein). Moreover, a large variety of MHD instabilities, among them the MRI, demand high numerical resolution, which is particularly hard to achieve in 3D models, and which adds to the computational demands that result from long evolution times on the one hand and severe time-step constraints set by high Alfvén speeds,  $v_A = B/\sqrt{4\pi\rho}$ , on the other. The exploration of magnetorotational explosions will therefore remain a challenging task for the coming years.

### E. Acoustic Mechanism

A new CCSN mechanism was envisioned in [108, 109] based on results of 2D hydrodynamic simulations, which did not yield explosions by neutrino-energy deposition. At late times after bounce ( $\gtrsim 1$  s), large-amplitude dipole ( $\ell = 1$ ) gravity-mode oscillations of the PNS core were found to be excited by SASI sloshing motions of the postshock layer and by anisotropic accretion downdrafts. The PNS vibrations (with amplitudes of several km) were damped by sending strong sound waves into the surrounding medium. Running down the density gradient away from the PNS the waves steepened into secondary shocks. The dissipation of the latter helped to heat the postshock region. Thus robust explosions were obtained for a variety of progenitors. For the conversion rate of accretion power,

$$\dot{E}_{\text{acc}} = \frac{GM_{\text{ns}}\dot{M}}{R_{\text{ns}}} \sim 1.3 \times 10^{52} \frac{\text{erg}}{\text{s}} \left( \frac{M_{\text{ns}}}{1.5 M_{\odot}} \right) \left( \frac{\dot{M}}{0.1 M_{\odot} \text{ s}^{-1}} \right) \left( \frac{30 \text{ km}}{R_{\text{ns}}} \right), \quad (15)$$

into acoustic power, one can estimate [108, 205]:

$$\begin{aligned} \dot{E}_{\text{sound}} &\sim \frac{\pi\rho}{2} (g_{\text{ns}}R_0)^{3/2} H_0^2 \\ &\sim 0.5 \times 10^{51} \frac{\text{erg}}{\text{s}} \rho_{11} g_{\text{ns},13}^{3/2} \left( \frac{R_0}{10 \text{ km}} \right)^{3/2} \left( \frac{H_0}{3 \text{ km}} \right)^2, \end{aligned} \quad (16)$$

(see also eq. 1 in [108]). Here,  $R_0$  is the accretion-stream radius,  $H_0$  the wave height,  $\rho_{11} = \rho/(10^{11} \text{ g/cm}^3)$  the average density at the “surface” of the PNS core, and  $g_{\text{ns},13} = g_{\text{ns}}/(10^{13} \text{ cm/s}^2)$  the average gravitational acceleration ( $g_{\text{ns}} = GM_{\text{ns}}/R_{\text{ns}}$ ) at the PNS “surface”. The reference value of  $\dot{E}_{\text{sound}}$  of Eq. (16) is suggestive. It exceeded the neutrino-energy deposition rate ( $\sim \tau(L_{\nu_e} + L_{\bar{\nu}_e})$ ; Sect. IV C 1) at late times in the numerical models. The violently vibrating PNS thus acted as a transducer channelling accretion energy efficiently into sound.

The fraction of the accretion power that is converted into core g-mode activity of the PNS could not be extracted reliably from the numerical calculations of [108, 109], thus leaving the value of  $H_0$  uncertain. Also final numbers for the explosion energies could not be determined, but the 2D explosions occurred very late, implying large NS masses and tending to be low-energetic. Fundamental questions about the excitation efficiency of the large-amplitude, low-order g-modes in the PNS remain to be answered, in particular whether 3D simulations would yield this phenomenon as well. So far other groups have not been able to reproduce the results (e.g., [106]), maybe because their models either were not evolved to sufficiently late times or exploded by neutrino heating before. A serious counterargument to the proposed scenario was made in [206]. Employing perturbation analysis the authors concluded that non-linear coupling between the low-order primary modes and pairs of high-order g-modes, whose small wavelengths cannot be resolved in hydrodynamical simulations, damps the low-order mode amplitudes to dynamically insignificant size. The thermalized pulsational energy is lost by neutrino emission.

## F. Phase-Transition Mechanism

A first-order hadron-to-quark matter phase transition that occurs at a sufficiently low density can have dynamical consequences during the postbounce accretion phase of the collapsing stellar core. This was discovered by [207, 208] using a hybrid EoS with a mixed phase that was softer than the hadronic phase and the pure quark phase. The latter was described by suitable choices of the parameters in the MIT bag model for strange (u,d,s) quark matter. Different from laboratory (heavy-ion collision) conditions, where the proton fraction  $Y_p$  is close to 0.5, the mixed phase appears at subnuclear densities for SN matter with  $Y_p \lesssim 0.3$ , and for all proton-to-baryon ratios shows a decrease of the transition density with higher temperatures. This is in contrast to other models for the hadron-quark phase transition, which predict an increase of the phase-transition density with increasing temperature (e.g., [209, 210]).

The very special properties of the hybrid EoS lead to gravitational instability of the PNS when it has accreted enough matter and has heated up during its contraction, entering the transition to quark matter in a growing dense-core region. The decrease of the effective adiabatic index there below the critical value for stability triggers a second, supersonic implosion to the denser pure quark phase, where the EoS suddenly stiffens again. This leads to considerable release of gravitational binding energy and the formation of a strong, second bounce shock, which catches up with the stalled primary shock to cause a SN explosion even in 1D models. When the second shock breaks out of the neutrinospheres,  $e^+$  captures by neutrons in the shock-heated matter emit a  $\bar{\nu}_e$  burst that may be detectable for a Galactic SN [211].

Though this is an interesting, new scenario, the fine tuning of the QCD phase transition is problematic. In particular, all EoS versions that lead to explosions so far are not compatible with the  $1.97 \pm 0.04 M_\odot$  NS mass limit of PSR J1614-2230 [124]. Changing the EoS parameters to reduce this inconsistency leads to a larger radius of the hybrid star and a less extreme density difference between hadronic and pure quark phases [208]. Whether SN explosions can be obtained with deconfinement scenarios compatible with PSR J1614-2230 still needs to be shown.

## V. OBSERVABLE SIGNALS FROM THE SUPERNOVA CORE

Neutrinos, gravitational waves, and heavy-element formation in the neutrino-heated ejecta are direct probes of the processes in the SN core. Because of the gain in sophistication of the models, in particular in the neutrino transport and by the inclusion of relativistic effects (recently also in 2D simulations), and because of the growing understanding of hydrodynamic instabilities during the postbounce accretion phase, interesting new aspects were discovered and are fit to change our notion of some of the accompanying phenomena and implications of CCSNe fundamentally.

### A. Neutrinos

Neutrinos and antineutrinos of all flavors radiated from the SN core (see production processes in Table I) carry information of the thermodynamic conditions (temperature, degeneracy) there, but also reflect dynamical processes associated with NS formation. A measurement of a neutrino signal from a future Galactic event could thus help to unravel the explosion mechanism.

The shock-breakout burst of  $\nu_e$  is a well known example of such a dynamical feature. It emerges when a flood of neutrinos freshly produced in shock-heated matter can suddenly escape when the bounce-shock reaches the neutrino-transparent regime at sufficiently low densities. Another example, though more on the exotic side, is the neutrino flash connected to the hadron-quark phase transition described in Sect. IV F. Also the pronounced rise of the mean energy of heavy-lepton neutrinos,  $\nu_x$ , when a PNS approaches collapse to a BH [212, 213] and possible —so far unclarified— signatures of magnetohydrodynamics can be mentioned here.

Moreover, the large-amplitude radial oscillations [80] or low-multipole (dipolar, quadrupolar) nonradial oscillations of the postshock layer (due to the SASI or due to convective activity for higher-multipole asymmetries) lead to quasi-periodic variations of the accretion flow to the PNS and to corresponding fluctuations of the accretion luminosity and mean energies of radiated neutrinos [214]. The effect is particularly strong for  $\nu_e$  and  $\bar{\nu}_e$ , for which a significant part of the luminosity (amounting to a fair fraction of the progenitor-specific accretion power, Eq. 15) originates from  $e^\pm$  captures on free nucleons in the hot accretion layer. In Fig. 7 these fluctuations are visible at  $t \gtrsim 100$  ms p.b. Note that the accretion luminosities depend strongly on the progenitor, and in both of the  $11.2$  and  $15 M_\odot$  models, accretion continues until the end of the simulated evolution simultaneously with the accelerating expansion of the shock (Fig. 6) and with the development of positive ejecta energy. Ongoing accretion is obvious because the  $\nu_e$  and  $\bar{\nu}_e$  luminosities are still considerably higher than those of  $\nu_x$ , whereas after accretion has ceased all luminosities become nearly equal (Fig. 5; [106, 107, 160]). The “luminosities” in the left panels of Fig. 7 are energy-loss rates,  $\dot{E}_\nu$ , of the PNS ( $\nu \in \{\nu_e, \bar{\nu}_e, \nu_\mu, \bar{\nu}_\mu, \nu_\tau, \bar{\nu}_\tau\}$ ) and not observable fluxes, the variation amplitudes are therefore damped by the

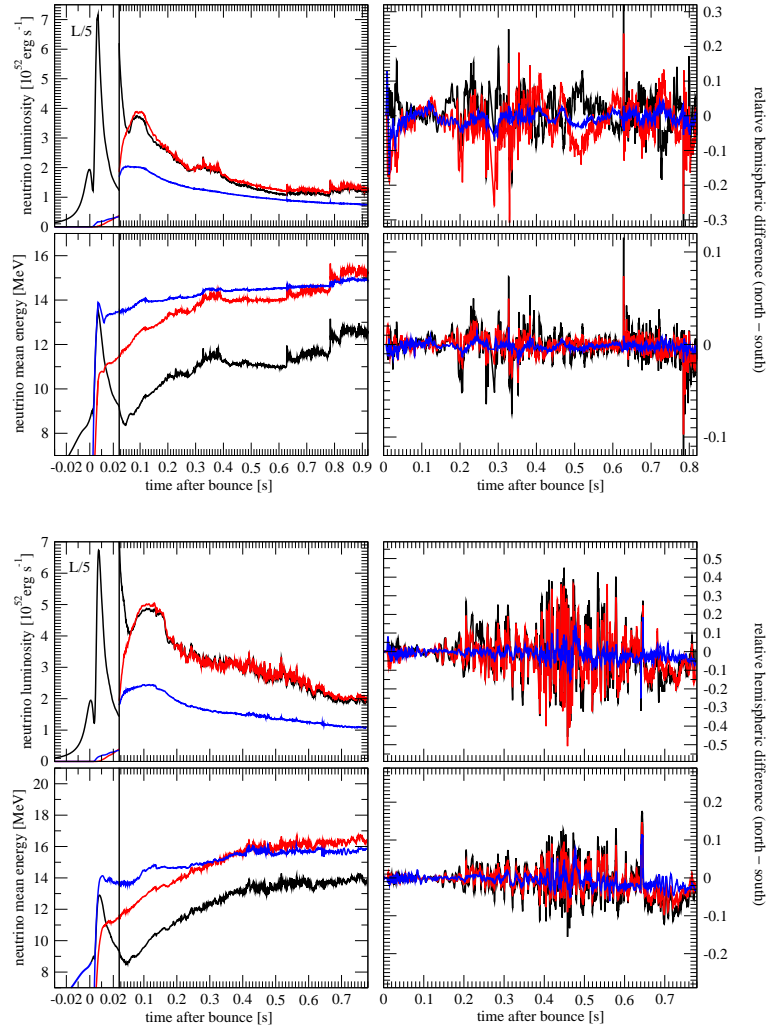


FIG. 7: Neutrino signals from general relativistic 2D simulations of core collapse and explosion of  $11.2 M_{\odot}$  (*upper plot*) and  $15 M_{\odot}$  (*lower plot*) stars shown in Fig. 6 [147]. The *left panels* of each plot show luminosities (i.e., total neutrino-energy loss rates of the PNS; *upper panels*) and mean energies (defined by the ratio of total neutrino energy-loss rate to number-loss rate,  $\dot{E}_{\nu}/\dot{N}_{\nu}$ ; *lower panels*) with black lines for  $\nu_e$ , red for  $\bar{\nu}_e$ , and blue for one kind of heavy-lepton neutrino  $\nu_x$ . The right panels display the corresponding relative hemispheric differences after core bounce (the infall remains spherical). All quantities are measured in the lab frame at large distance. Note that the fluctuations, sudden jumps, and north-south differences at  $t > 300$  ms in the upper plot are caused by violent, time-dependent, anisotropic downflows and corresponding changes of the accretion rate of the PNS.

integration over all directions, and their true magnitude (percents to tens of percents) can be better read off the right panel, where relative hemispheric differences are displayed.

The SASI and convective modulation of the neutrino emission was not only seen in 2D simulations with RbR neutrino transport, but also with multi-angle treatment ([112]; cf. Sect. III B for a discussion of methods). It may be detectable for a Galactic SN at a fiducial distance of 10 kpc with IceCube or future megaton-class instruments [215]. First 3D simulations with approximative neutrino transport suggest that the variation amplitudes could be smaller than in 2D [96], but more and better 3D models with multi-group transport are needed for reliable information.

Another remarkable property of the neutrino signals in Figs. 5 and 7 is the close similarity and even crossing of the mean energies of  $\bar{\nu}_e$  and  $\nu_x$  [107, 214]. Instead of the previous notion that  $\nu_x$  are significantly more energetic than  $\nu_e$  and  $\bar{\nu}_e$ , i.e., instead of a neutrino-energy hierarchy of  $\langle \epsilon_{\nu_e} \rangle < \langle \epsilon_{\bar{\nu}_e} \rangle < \langle \epsilon_{\nu_x} \rangle$  with typically  $\langle \epsilon_{\nu_x} \rangle \gtrsim 18$ –20 MeV, state-of-the-art models now yield  $\langle \epsilon_{\nu_e} \rangle < \langle \epsilon_{\bar{\nu}_e} \rangle \sim \langle \epsilon_{\nu_x} \rangle$  and  $\langle \epsilon_{\nu_x} \rangle \lesssim 13$ –16 MeV (Figs. 5, 7, and ref. [214]; also ref. [79], where rms energies are given, however). The exact value depends on the time and EoS: A softer EoS lead to a more compact and hotter PNS and thus higher mean energies [214].

While during the later accretion phase the order of  $\langle \epsilon_{\bar{\nu}_e} \rangle$  and  $\langle \epsilon_{\nu_x} \rangle$  can be reversed (Fig. 7), one obtains a mild

hierarchy  $\langle \epsilon_{\bar{\nu}_e} \rangle < \langle \epsilon_{\nu_x} \rangle$  during the PNS cooling phase (Fig. 5), which, however, diminishes to insignificant differences at very late times (seconds after bounce), where the mean energies of all neutrino kinds become nearly identical,  $\langle \epsilon_{\nu_e} \rangle \approx \langle \epsilon_{\bar{\nu}_e} \rangle \approx \langle \epsilon_{\nu_x} \rangle$  (Fig. 5, [107, 216]). The late behavior can be understood by the flat temperature profile inside the PNS during the late cooling stage and the close proximity of the neutrinospheric positions of all neutrinos then. This proximity is caused by the strong dominance of neutral-current scatterings in the effective opacity (i.e., inverse mean free path) for thermal coupling between neutrinos and stellar medium,  $\kappa_{\text{eff}} \equiv \sqrt{\kappa_e(\kappa_s + \kappa_e)}$  ( $\kappa_e$  and  $\kappa_s$  being the opacities for neutrino-production processes and nucleon scatterings, respectively) at conditions where  $e^-$  are strongly degenerate and neutrons start to become degenerate [216]<sup>4</sup>. The close similarity of  $\langle \epsilon_{\nu_x} \rangle$  and  $\langle \epsilon_{\bar{\nu}_e} \rangle$  during the early postbounce and accretion phases is fostered by nucleon-nucleon-bremsstrahlung as main  $\nu_x$  production channel [220], because it shifts the energy-sphere of  $\nu_x$  to lower temperature [221]. However, the effect is considerably enhanced (compare the two cases discussed in [107]) by energy losses of  $\nu_x$  in collisions with free nucleons  $N = n, p$  (“inelastic” —better “non-conservative”— nucleon recoil; Table I). Such losses occur when the neutrinos diffuse out through the (optically) thick scattering layer between energy- and transport-spheres [221, 222]. The small but very frequent energy transfers with an average value per collision of  $\langle \Delta \epsilon_{\nu} \rangle_{\nu N} \sim \epsilon_{\nu}(6 k_B T - \epsilon_{\nu})/(m_N c^2)$  [223] can force the  $\nu_x$ -spectrum to become even softer than that of  $\bar{\nu}_e$ , whose production in a hot accretion layer by  $e^+$  captures on neutrons is very efficient.

The close similarity of the spectra of all neutrinos and the corresponding relevance of non-conservative nucleon recoils, which is still widely ignored, have a bearing on the consequences of neutrino-flavor conversions, e.g., the rise time of the detectable  $\bar{\nu}_e$  signal [224], and on neutrino-induced or flavor-oscillation dependent r-process nucleosynthesis in SNe [225, 226]. Also the steep rise of  $\langle \epsilon_{\nu_x} \rangle$  before BH formation, which was found without taking non-conservative nucleon recoils into account [212, 213], may be affected.

## B. Gravitational Waves

Any nonspherical, accelerated mass motions in the SN core act as source of GWs, whose amplitude at a source distance  $D$  scales with the second derivative of the mass-quadrupole moment,  $h \sim (2G/c^4)(\ddot{Q}/D)$ . The GW signal reflects the activity phases partly visible also in the neutrino-luminosity variations (compare Figs. 7 and 8). Convective overturn caused by negative entropy gradients in the deceleration region of the bounce shock and in the neutrino-heating layer, the violent SASI sloshing of the whole postshock volume, and the impact of accretion downdrafts, which occur even after the onset of the explosion, induce surface g-modes in the outer layers of the PNS [214], whose frequency determines that of the GW emission [227]. Because the buoyancy (Brunt-Väisälä) frequency connected to the gravity waves depends on the compactness of the PNS (see text following Eq. 3), not only the stiffness of the EoS has a big influence [214] but also GR gravity is crucial to predict the GW spectrum, which for relativistic models peaks around 800–1000 Hz while Newtonian simulations yield significantly lower frequencies [147].

GWs are expected to carry characteristic signatures of the explosion mechanism. While wave components associated with long-lasting convective and SASI activity and a broad-band signal seem typical of neutrino-driven explosions, the large-amplitude g-mode oscillations of the PNS core, which are essential for the acoustic mechanism, would lead to a dramatic rise of the GW amplitude shortly before the blast sets in [228]. In contrast, rapid stellar core rotation as required for MHD explosions would produce a powerful GW burst at core bounce, possibly followed by postbounce emission due to triaxial instabilities [18].

The GW features and activity phases seen in 2D models are also found in 3D simulations, though the amplitudes may be different. Without symmetry constraints, however, the detailed signal structure varies strongly with the observer direction and does not possess any template character [93, 147, 229, 230].

## C. Heavy Elements

Besides reprocessing shock-heated stellar layers by explosive burning, nucleosynthesis takes place in the neutrino-heated ejecta from the close NS vicinity. The ejecta consist of two components and have great potential for diagnostics of the SN mechanism.

The first component consists of the early ejecta from the phase of shock revival. Its composition at freeze-out depends on the expansion timescale, which is intrinsically linked to the blast dynamics and thus to the explosion

---

<sup>4</sup> For the influence of the EoS-specific nucleon potential energies in dense NS matter, which affect the  $\beta$ -processes of  $\nu_e$  and  $\bar{\nu}_e$  but were ignored in the models of Figs. 5 and 7, see refs. [217–219].

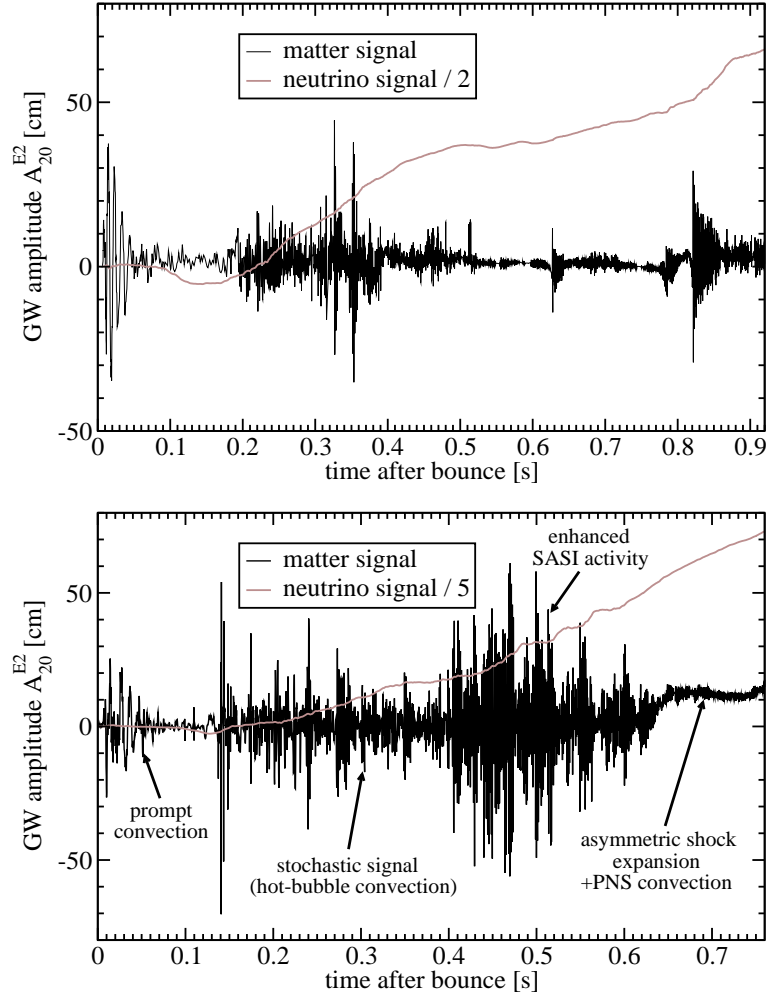


FIG. 8: Amplitudes of gravitational waves (GWs) from the general relativistic 2D simulations of core collapse and explosion of  $11.2 M_{\odot}$  (*upper plot*) and  $15 M_{\odot}$  (*lower plot*) stars shown in Fig. 6 [147]. The light brown lines (scaled down by factors of two and five in the upper and lower panel, respectively) display the growing amplitude connected with the asymmetric neutrino emission. The matter signal (solid black line) exhibits activity phases associated with strong, prompt postbounce convection (for  $t_{\text{pb}} \lesssim 50$  ms), increasingly violent convective and SASI mass motions in the postshock layer before the explosion sets in (between  $\sim 100$  ms and 350 ms (500 ms) in the  $11.2 M_{\odot}$  ( $15 M_{\odot}$ ) case), and the continued impact of asymmetric accretion downdrafts on the PNS after the launch of the explosion. The non-zero value of the matter signal at late times is a consequence of the aspherical expansion of the shocked ejecta.

mechanism, but it also depends on the neutron-to-proton ratio set by the competition of  $e^{\pm}$  captures on nucleons and the inverse  $\nu_e$  and  $\bar{\nu}_e$  captures (top two beta-processes in Table I).

A good example for the relevance of these effects are recent 2D results of ONeMg-core explosions, where acceleration by convective buoyancy expulses early ejecta so rapidly that this material is able to retain a neutron excess sufficient for weak r-processing, in contrast to 1D models where beta-reactions in the more slowly ejected plasma lift  $Y_e$  close to 0.5 and above [33]. It will be interesting to explore the combination of composition and asymmetry differences of the early ejecta in magnetorotational explosions compared to neutrino-driven ones when eventually self-consistent, well resolved multi-dimensional MHD models with sophisticated neutrino transport (instead of no or highly simplified neutrino treatment) become available.

The second component is the neutrino-driven wind blown off the surface of the hot PNS by neutrino-energy deposition above the neutrinosphere after the explosion has been launched. The properties of this—in the absence of rotation and/or strong magnetic fields—essentially spherically symmetric outflow depend on the strong gravity field of the NS and on the properties (luminosities and spectra) of the radiated neutrinos, which determine the strength of the heating [231, 232]. Again the beta-processes of free nucleons (Table I) set the  $n/p$  ratio of this environment. For sufficiently high entropy and sufficiently large neutron excess this wind may provide an interesting site for r-process

nucleosynthesis [233].

However, besides the long-standing problem of insufficient entropy [234, 235], sophisticated hydrodynamic models find the wind to be proton-rich [107, 160]. This is a consequence of the close similarity of the spectra and luminosities of  $\nu_e$  and  $\bar{\nu}_e$  during the PNS cooling phase,  $L_{\bar{\nu}_e} \approx L_{\nu_e}$  and  $\langle \epsilon_{\bar{\nu}_e} \rangle \approx \langle \epsilon_{\nu_e} \rangle$  (Fig. 5 and Sect. V A), which enforces  $Y_e > 0.5$ . Since [231]

$$Y_e \sim \left[ 1 + \frac{L_{\bar{\nu}_e}(\epsilon_{\bar{\nu}_e} - 2\Delta)}{L_{\nu_e}(\epsilon_{\nu_e} + 2\Delta)} \right]^{-1} \quad (17)$$

with  $\epsilon_\nu = \langle \epsilon_\nu^2 \rangle / \langle \epsilon_\nu \rangle$  and  $\Delta = (m_n - m_p)c^2 \approx 1.29 \text{ MeV}$ , values of  $Y_e < 0.5$  require considerably more energetic  $\bar{\nu}_e$  than  $\nu_e$ , satisfying  $\epsilon_{\bar{\nu}_e} - \epsilon_{\nu_e} > 4\Delta$ . Recently it was shown that the nucleon potential energies in dense NS matter, connected to the nuclear symmetry energy, may cause sufficiently large spectral differences of  $\nu_e$  and  $\bar{\nu}_e$  to bring the wind  $Y_e$  slightly below 0.5 [217–219]. But it still needs to be seen whether this reduction allows for an r-process.

A dominance of protons prevents r-processing but might enable a  $\nu p$ -process [236, 237]. Active-sterile  $\nu_e$ - $\nu_s$  conversions involving a possible sterile neutrino  $\nu_s$  in the eV-mass range, as suggested by an anomaly of reactor  $\bar{\nu}_e$  spectra and their distance and energy variation, can decrease the proton excess by removing  $\nu_e$  and thus suppressing their absorption on neutrons. A recent investigation based on an ECSN model, however, revealed only a modest effect, insufficient for an r-process [238]. But the results depend in a complex way on the interplay between  $\nu_e$ - $\nu_s$  MSW matter oscillations and collective  $\nu\bar{\nu}$  flavor conversion, which strongly reduces the pure matter effect. More exploration seems necessary.

## VI. EXPLOSION PROPERTIES AND COMPACT REMNANTS

The explosion mechanism establishes the link between progenitor stars and SNe and their remnants. It is therefore natural to seek for observables that might provide indirect evidence of the processes triggering the onset of the blast. In the following the implications and limitations of neutrino-driven explosions will be briefly discussed with respect to pulsar kicks, SN asymmetries, and progenitor-dependent explosion and remnant properties.

### A. Pulsar Kicks and Spins

Young pulsars are observed to possess average space velocities around 400 km/s, some of them even more than 1000 km/s [242]. This is too high to be understood by the breakup of binary systems in SN explosions, and natal kicks of the NSs are required [243].

An asymmetric initiation of the explosion can naturally impart a recoil velocity to the NS due to linear momentum conservation. Impulsive momentum transfer by hydrodynamic forces of anisotropically expelled gas during the convective launch phase of the explosion, however, is hardly able to account for more than  $\sim 200$  km/s even in the most optimistic case [244]. Therefore a strong unipolar asymmetry in the progenitor star prior to collapse—in contrast to the higher-multipole asymmetries usually resulting from the stochastic and chaotic growth of hydrodynamical instabilities seeded by small, random perturbations (Sect. IV C 3)—has been hypothesized to define a preferred direction in which the SN blast could break out with the highest velocities [245, 246]. However, stellar evolution models, self-consistently evolved in 3D through all advanced burning stages up to gravitational instability, which could lend convincing support to the existence of such global, low-multipole pre-collapse asymmetries, do not exist yet.

Anisotropic neutrino emission is another potential NS kick mechanism by which the NS could achieve a recoil velocity of  $v_{\text{ns}} \sim \xi_\nu \cdot 33000 \text{ km/s} (E_\nu/3 \times 10^{53} \text{ erg})(M_{\text{ns}}/1.5 M_\odot)^{-1}$ . An asymmetry  $\xi_\nu$  of 1% of the total neutrino energy loss would thus kick the NS to more than 300 km/s. The asymmetric neutrino emission associated both with postbounce accretion [94, 95] and with the convective activity during the PNS cooling evolution [157], however, is highly time variable and nonstationary in space and time; therefore, it can hardly account for recoil velocities of more than 10 km/s. Exotic mechanisms, invoking ultrastrong NS magnetic dipole fields and non-standard, still uncertain neutrino properties have therefore been suggested as speculative solution (e.g., [247] and refs. therein).

Probably the most plausible origin of the NS velocities was proposed on the basis of 2D explosion simulations by Scheck et al. [94, 248], whose results received recent confirmation by 2D [249, 250] and 3D models [95, 239]. Scheck et al. showed that the asymmetric expulsion of gas does not only exert “contact forces” during a few 100 ms, in which the explosion is launched and ejecta and PNS interact hydrodynamically, but that the asymmetric ejecta exert a long-time, anisotropic gravitational pull, which can accelerate the PNS over seconds to velocities of many 100 km/s (Fig. 9). For particularly large asphericity of the ejecta a NS velocity of  $v_{\text{ns}} > 1000 \text{ km/s}$  was obtained [94]. A hemispheric



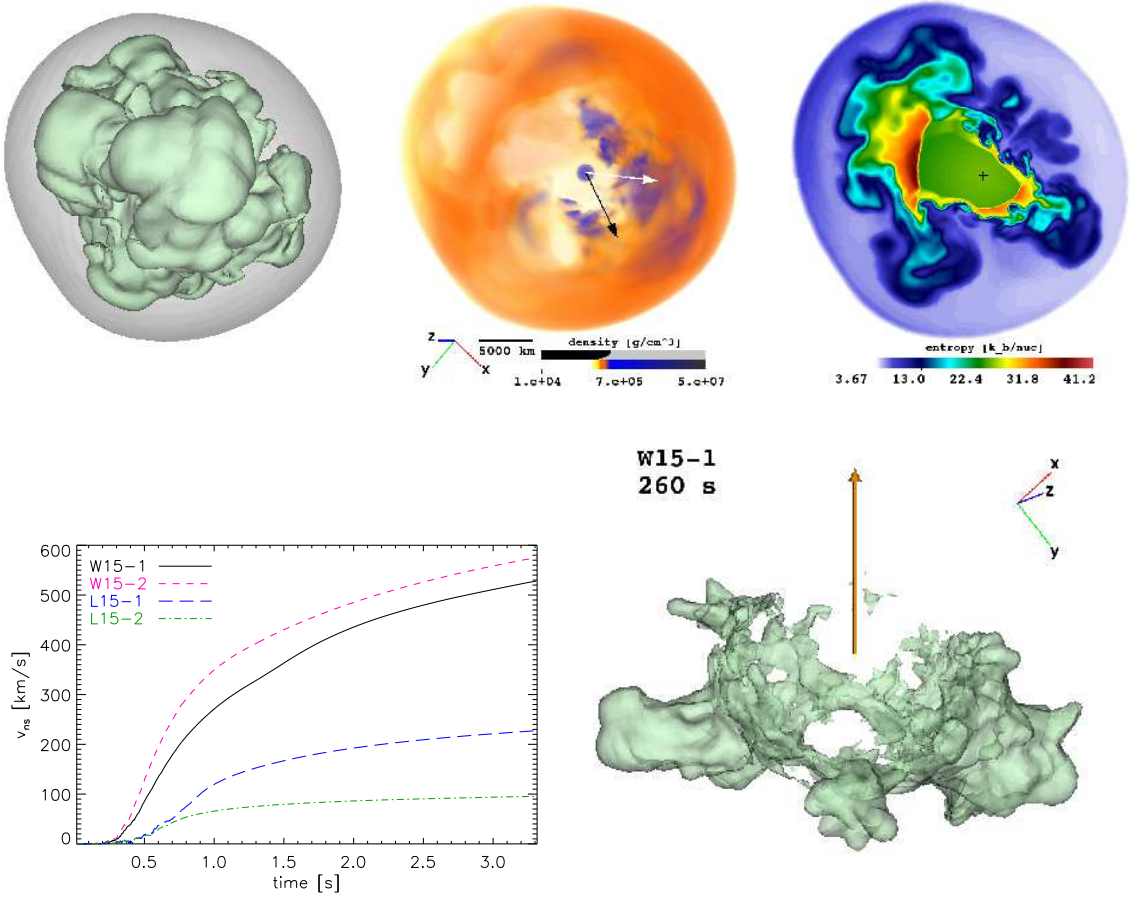


FIG. 9: NS kicks and anisotropic Ni ejection for asymmetric SN explosions in 3D simulations [95, 239]. *Upper panels:* Entropy isosurfaces of SN shock and convective bubbles (*left*) and ray-casting image of the density (*middle*) at  $t = 1.3$  s after bounce. The deformed boundary is the shock, the viewing direction is normal to the plane of NS kick and spin vectors (white and black arrows), which define the plane of the entropy distribution (*right*). The NS (black cross) is clearly displaced from the geometrical center of the expanding shock towards the side of weaker explosion. It is accelerated mainly by the asymmetric gravitational attraction of less rapidly expanding, dense ejecta clumps (intense reddish and bluish in middle image). *Left lower panel:* Recoil velocity of the NS vs. time for four 3D explosion simulations of different stars. The acceleration continues even later than 3 s and kicks of  $>600$  km/s are reached. *Right lower panel:* Anisotropic production of radioactive  $^{56}\text{Ni}$  by explosive nuclear burning behind the expanding shock. For large NS kicks nickel is ejected preferentially in the direction where the shock is stronger, i.e., opposite to the NS motion (red arrow).

asymmetry of the mass distribution of only  $\Delta m = \pm 10^{-3} M_{\odot}$  in a shell expanding away from the NS from an initial radius  $r_i = 100$  km with  $v_s = 3000$  km s $^{-1}$  can tug the NS to a velocity of  $v_{\text{ns}} \approx 2G\Delta m/(r_i v_s) \approx 900$  km s $^{-1}$  [95, 239].

Gravitational forces of anisotropically ejected gas can thus mediate an efficient, long-lasting acceleration of the NS, transferring momentum from the anisotropically ejected matter to the compact remnant. Since the NS is gravitationally pulled by the slower, usually denser ejecta associated with a weaker explosion shock, Wongwathanarat et al. [239] expect the bulk of the iron-group nuclei and of other elements heavier than  $^{28}\text{Si}$ , which are explosively produced in the shock-heated ejecta, to be expelled preferentially in the direction opposite to the NS motion. They predict a very strong asymmetry of the nickel ejection in the case of large NS kicks (see Fig. 9), which could be an observationally accessible, characteristic feature of the hydrodynamical-gravitational kick mechanism.

Asymmetrical convective downdrafts and rising bubbles as well as violent, low-multipole SASI sloshing modes, which have spiral components in 3D, can establish angular momentum separation between PNS and ejecta and thus may cause considerable PNS rotation even if the stellar core did not rotate before collapse ([82, 83]; because of the use of an inner boundary condition, however, these results were questioned by [251]). Naturally, any anisotropic mass infall that hits the accretor not exactly head-on can exert a torque and spin up the PNS. A mass  $\Delta m = 10^{-3} M_{\odot}$  that has an impact velocity  $v_{\text{imp}} \sim \sqrt{2GM_{\text{ns}}/R_{\text{ns}}} \sim 10^{10}$  cm/s and an impact parameter  $d \equiv \zeta R_{\text{ns}} \sim 30$  km when colliding with the NS transfers an angular momentum of  $\Delta J_{\text{ns}} = \Delta m v_{\text{imp}} d \sim 6 \times 10^{46}$  g cm $^2$ /s, corresponding to a NS spin period of  $T_{\text{ns}} = 2\pi I_{\text{ns}}/\Delta J_{\text{ns}} \sim 0.2$  s for a typical value of the NS moment of inertia of  $I_{\text{ns}} \sim 2 \times 10^{45}$  g cm $^2$ .

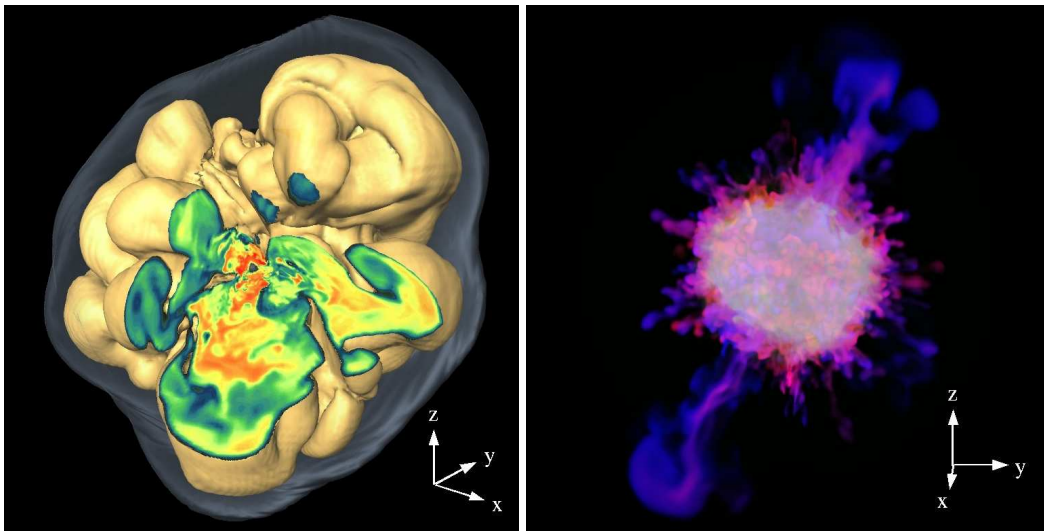


FIG. 10: *Left panel:* Asymmetric shock front (outer bluish, nearly transparent surface) and mushroom-like, high-entropy bubbles of neutrino-heated plasma around the central NS (dark grey surface near the middle) at 0.5 s after bounce in a 3D SN simulation [240]. The shock front has a diameter of  $\sim 4000$  km. An octant is cut out to show the entropy distribution (color-coded between  $\sim 10$  and  $21 k_B$  from blue to yellow to red) in the expanding Rayleigh-Taylor mushrooms surrounded by cooler accretion downdrafts. All visible structures have grown from tiny, random seed perturbations by hydrodynamic instabilities. *Right panel:* Asymmetric ejection of different chemical elements during the explosion of the left image, but  $\sim 9000$  s later into the SN evolution [240]. The side length of the displayed volume is about  $7.5 \times 10^7$  km. The largest bubbles on the left image have seeded the growth of the most prominent Rayleigh-Taylor fingers in the right picture, which expand with up to 4500 km/s. They are surrounded by the helium and hydrogen of the outer stellar shells (not visible). Together with the smaller features they thus carry heavier chemical elements from deep stellar layers far into more slowly expanding, lighter SN material. Blue filaments contain dominantly nickel, red fingers mostly oxygen, and green is associated with carbon. A mix of nickel and oxygen appears in pink. The whitish glow results from a contamination with other colors as a consequence of the volume rendering for the visualization.

Indeed, 3D explosion simulations yield  $T_{\text{ns}}$  in the range of hundreds of milliseconds to seconds [95, 239]. Nevertheless, angular momentum transferred to the PNS by hydrodynamical flows during the development of the explosion and in the post-explosion accretion phase is unlikely to be sufficient to account for the estimated NS birth spin periods of order  $\sim 10$  ms, which seems to require rotation of the collapsing stellar core [36, 252]. Explaining a possible spin-kick correlation of observed NSs remains a challenge for any discussed kick mechanism connected to explosion asymmetries of progenitor stars with or without rotation.

## B. Supernova Asymmetries

The large asymmetries imprinted on the ejecta by the violent, nonradial mass motions in the SN core, which precede and accompany the neutrino-driven revival of the blast wave, seed the growth of secondary Rayleigh-Taylor instability in the shock-accelerated outer shells of the exploding star [253]. Since the developing Rayleigh-Taylor mushrooms are denser than the surrounding gas, they are less decelerated than their environment and can penetrate the composition interfaces of the progenitor, retaining high velocities as the SN ejecta expand. Thus they carry freshly synthesized radioactive nickel and other heavy elements from the vicinity of the nascent NS into the outer stellar layers. Significant amounts of the initially innermost ejecta can be mixed deep into the helium shell and even the hydrogen layer of the disrupted star [254], destroying the well-stratified onion-shell structure of the progenitor.

In 3D simulations of a SN 1987A progenitor model, large nickel-dominated clumps (containing up to several  $10^{-3} M_{\odot}$  of  $^{56}\text{Ni}$ ) were found to speed through the stellar hydrogen envelope with up to 4500 km/s (Fig. 10; [240]). This can explain mixing phenomena and asymmetries observed in SN 1987A, e.g. the detection of X-rays and  $\gamma$ -rays from the radioactive nickel decay much earlier than predicted by 1D explosion models [69]. The outward mixing of radioactive nickel and inward displacement of hydrogen can well account for the shape and width of the lightcurve maximum of SN 1987A (V. Utrobin, private communication).

However, it is still unclear whether explosion asymmetries associated with the development of hydrodynamic instabilities in the SN core and the subsequent growth of mixing instabilities in the stellar envelope are able to explain the

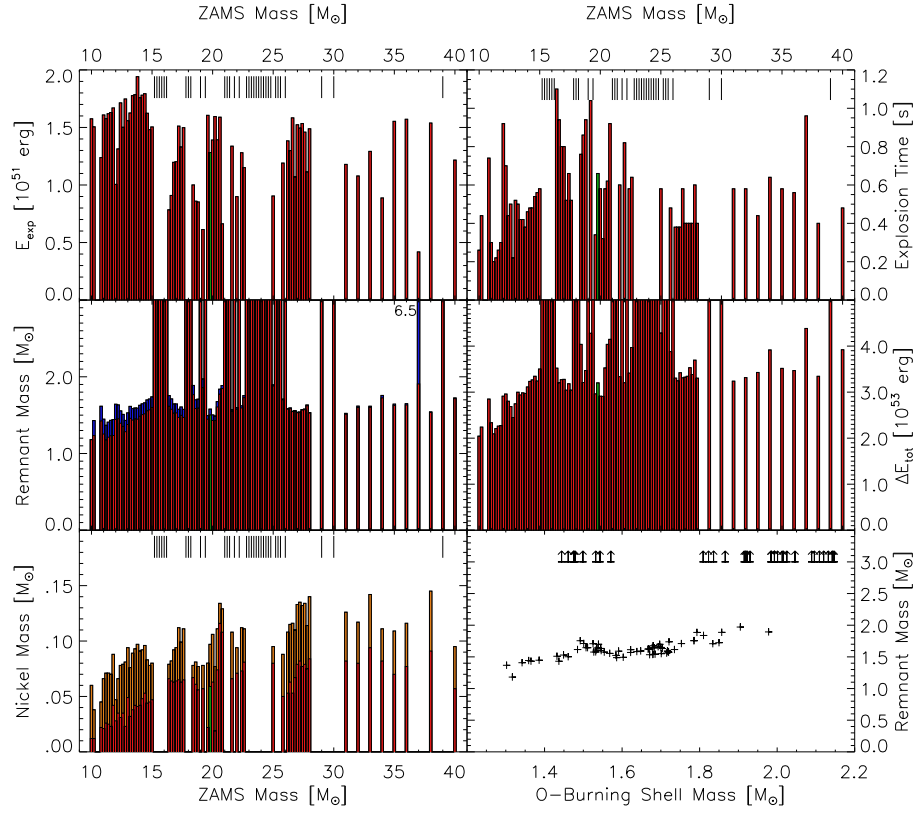


FIG. 11: Explosion and remnant properties predicted by parametrized 1D neutrino-driven SN simulations [241] of a large set of progenitor stars from [22]. Explosion energy (*top left*), time of onset (*top right*), baryonic remnant mass (*middle left*), neutrino-energy release by the compact remnant (*middle right*), and ejected Ni mass (*bottom left*) are shown as functions of stellar birth (ZAMS) mass. The lower right plot gives the compact remnant mass vs. the enclosed mass at the base of the O-burning shell of the progenitor. Neutrino cooling of the dense NS core was prescribed such that the properties of SN 1987A were roughly reproduced for  $\sim 20 M_{\odot}$  stars (green histogram bar). Accretion neutrino luminosity was self-consistently computed by approximate neutrino transport. The ticks in some panels mark masses where computed models did not explode. Bars of remnant masses reaching to the upper panel edge ( $3 M_{\odot}$ ) and arrows in the bottom right panel signal formation of a BH containing the whole mass of the star at collapse. The only exception is the  $37 M_{\odot}$  progenitor, where the explosion ejects  $\sim 3.2 M_{\odot}$  while fallback creates a BH with  $6.5 M_{\odot}$ . Blue segments indicate fallback masses and orange segments Ni-mass uncertainties because of unclear Ni abundance in the  $\nu$ -heated ejecta.

prolate shape of the SN 1987A ejecta cloud. It will also have to be seen whether they can account for the extremely fast “jet” structures observed ahead of the explosion shock in the Cassiopeia A SN remnant. Moreover, the global asphericity of most SNe Ib/c might require larger nonradial deformation than the asymmetric structures that can stochastically grow from initially small random perturbations.

### C. Neutron Stars and Black Holes

Remnant masses and explosion properties (energy, ejected  $^{56}\text{Ni}$  mass) and their systematics with the progenitor mass also carry information on the explosion mechanism. The observational basis of determined or constrained NS and BH masses [125, 255, 256], SN-progenitor connections [26, 27], and estimated explosion parameters (e.g., [24, 25]; Fig. 3) is rapidly growing.

From the observed mass distribution of compact remnants and its possible gap between  $\sim 2$  and  $5 M_{\odot}$  at the boundary between NSs and BHs, it was inferred that the SN engine must launch the (neutrino-powered) explosion within 100–200 ms after bounce in order not to overproduce remnants in the gap [257, 258]. This was considered as argument that the mechanism is supported by Rayleigh-Taylor (convective) rather than SASI instability. However, in the SN core both of these nonradial instabilities occur simultaneously [76, 161] and cannot be separated just on the basis of a timescale argument. Moreover, the population evolution models of [257, 258] used very simple theoretical considerations to determine the explosion energy for early and late explosions and to estimate the fallback mass of

matter that initially moves outward but ultimately fails to escape because of insufficient blast-wave energy. The analytic theory ignores, for example, dynamical effects and the nonnegligible additional power carried by the early neutrino-driven wind (cf. [94]). Other approaches to predict mass distributions of NSs and/or BHs were based either on piston-driven explosions with predefined mass cut and explosion energy (e.g., [259]), or on a single-parameter criterion to distinguish progenitors that are likely to explode or not [260].

In [241] an alternative approach was adopted. Hydrodynamical simulations in 1D were performed for a large set (roughly 100) of solar-metallicity progenitors of [22] using an analytic, time-dependent two-zone model of the cooling, contracting PNS, whose free parameters were calibrated such that the explosion energy and  $^{56}\text{Ni}$  mass of SN 1987A were reproduced for stars with ZAMS mass around  $20 M_{\odot}$ . The effects of accretion luminosity were taken into account by simplified neutrino transport [94]. With this prescription all stellar collapses and possible explosions were simulated for at least 15 s beyond core bounce and were followed after the PNS cooling for hours to days later until the fallback mass was determined.

Results of the calculations are shown in Fig. 11 and reveal a number of interesting insights, which, of course, depend on the considered progenitor set:

- Because the stellar structure varies nonmonotonically, the SN properties depend on the progenitor mass in a complex way. Large differences of the explosion characteristics are possible for small mass differences.
- Failed explosions with BH formation seem possible for progenitors below  $20 M_{\odot}$ , and successful SNe with NS formation are found also between 20 and  $40 M_{\odot}$ .
- Neutrino-driven explosions with energies in excess of  $2 \times 10^{51}$  erg and  $^{56}\text{Ni}$  production of significantly more than  $\sim 0.1 M_{\odot}$  seem unlikely.
- The time of the onset of the SN blast (measured by the moment the shock passes 500 km) varies between  $\sim 0.1$  s and 1.1 s, so it includes “early” and “late” cases. Later explosions tend to be less energetic because less mass is available for being heated by neutrinos.
- The NS baryonic masses are in the range of  $\sim 1.2$ – $2 M_{\odot}$ . The smallest BH, formed by fallback, contains  $6.5 M_{\odot}$ , all other BHs originate from failed explosions and contain all the mass of the progenitor at collapse ( $> 8.5 M_{\odot}$ ). The possible gap of the observed remnant distribution is clearly reproduced.
- Fallback is larger for the lower-mass progenitors where an extended hydrogen envelope leads to a stronger reverse shock. The result of little fallback in solar-metallicity progenitors is compatible with conclusions drawn from an analysis of observed double NS systems [261].
- Although the remnant mass is an almost monotonic function of the enclosed mass at the base of the oxygen-burning shell, the latter is no reliable indicator for the fate of the star because some models with relatively small Si-cores do not explode.
- Neutrino-driven explosions are fostered by big “jumps” in the stellar density and entropy profiles (cf. Fig. 2), reducing the mass-infall rate (and ram pressure) and allowing the shock to expand (cf. Eq. 2).

Certainly these results are based on 1D simulations and many approximations were made. Therefore they can be only a very first step, but nevertheless are enlightening concerning the implications of neutrino-powered explosions. They challenge a number of paradigms for the progenitor-explosion and progenitor-remnant connections. In particular the limited blast-wave energy and nickel production support arguments in favor of another explosion mechanism for HNe. These events are likely to be triggered by magnetorotational processes. More research, observationally and theoretically, will have to clarify whether there is a continuous transition between both, associated with a varied degree of progenitor rotation and leading to a continuous spectrum of explosion energies that reach from the neutrino-powered regime of  $E_{\text{exp}} \lesssim 2 \times 10^{51}$  erg to the hyperenergetic regime of  $E_{\text{exp}} > 10^{52}$  erg as suggested by some phenomenological studies (see Fig. 3).

## VII. SUMMARY, CONCLUSIONS, OUTLOOK

Supernova theory has made remarkable progress over the past decade, promoted by common interests of the astro-, particle (neutrino), nuclear, and gravitational physics communities and by an increasing number of active (young) researchers in the field. A deeper understanding of the physical mechanisms that initiate and fuel SN and HN explosions of massive stars is of crucial importance not only for establishing the progenitor-remnant connection but

also for predicting the properties of stellar explosions, their nucleosynthetic output, and the characteristics of their gravitational-wave and neutrino signals.

The most sophisticated present simulations demonstrate that neutrino-energy deposition can power ECSNe (even in spherical models) of  $\sim 9 M_{\odot}$  stars with ONeMg-cores near the lower mass limit for SN progenitors (Fig. 5). Overall, the features of such explosions, e.g., low energy and little nickel production, seem to be compatible with observational candidates like the Crab SN and some faint transients. Multi-dimensional simulations suggest these explosions to be potential sources of light r-process nuclei up to silver and palladium (Sect. V C). Several groups have also reported successful neutrino-driven explosions (with multi-group neutrino transport) for Fe-core progenitors above  $10 M_{\odot}$  (Sect. IV C 2; Figs. 4, 5). Ultimate confirmation of the viability of this mechanism for a wider range of progenitor masses therefore seems to be in reach.

The onset of the explosion can be understood as a global runaway instability of the accretion layer, whose initiation depends on the power of neutrino-energy deposition. While the exact mode of the runaway is still a matter of exploration and debate (e.g., low-multipole SASI or higher-multipole convective, oscillatory or nonoscillatory?), its threshold in terms of the driving neutrino luminosity is lowered by nonradial fluid motions in the neutrino-heating layer. Such flows play a supportive role because they stretch the residence time of matter in the gain region and thus decrease the heating timescale and increase the efficiency of neutrino-energy deposition, leading to successful explosions even when sophisticated spherical models fail (Sect. IV C 3). The efficiency of neutrino-energy transfer, the growth conditions and growth rates of different hydrodynamic instabilities, and the critical luminosity threshold for an explosion may not only depend on the dimension and thus will ultimately require simulations in 3D, but have been shown to depend also on putative “details” of the physics ingredients like approximations for the energy and velocity dependence of the neutrino transport, the neutrino-interaction rates, general relativity, and the contraction of the nascent NS in response to the nuclear EoS (Sect. III; Fig. 4). Moreover, the outcome of the complex neutrino-hydrodynamical simulations can be sensitive to the numerical resolution, which naturally is subject to limitations in full-scale, multi-dimensional SN-core models.

While detailed modeling of the processes in collapsing stars now pushes forward from the second to the third dimension, facing considerable computational challenges and demands mainly for the neutrino transport, a growing host of studies begins to explore the observational consequences of neutrino-driven explosions. In view of existing and upcoming big detection facilities, in particular neutrino and gravitational-wave signals (Figs. 5, 7, 8) are of relevance for SN-core diagnostics targeting a future Galactic SN. The former even have the potential to yield valuable information on particle properties of the neutrinos provided the characteristics of the SN emission are sufficiently well understood (e.g., [224, 262–264]). Sophisticated neutrino transport and interaction treatments have revealed interesting signal features like an amazing robustness of the neutronization  $\nu_e$  burst [262], characteristic differences of the rise time of the  $\bar{\nu}_e$  and  $\nu_x$  emission after bounce [224], luminosity variations associated with nonsteady flows in the accretion layer [112, 214], and a close similarity of the luminosities and spectra of neutrinos and antineutrinos of all flavors during the PNS cooling phase (Sect. V A, Fig. 5; [107, 216]) with important consequences for SN nucleosynthesis (Sect. V C).

While a Galactic SN in the near future is a realistic possibility, it will be a unique event and might not provide evidence of wider validity. Photometric and spectroscopic diagnostics of extragalactic SNe and of gaseous, young SN remnants, which reveal information on explosion energies,  $^{56}\text{Ni}$  production, ejecta masses, asymmetries, and composition, as well as progenitor constraints (cf. Fig. 3) are therefore extremely valuable, and more is desirable. First-principle explosion models begin to become mature enough to be linked to such observations, a possibility that defines a fruitful territory for future research. Neutrino-driven explosion models also begin to allow for predictions of compact remnant (NSs and BHs) masses, kicks, and spins.

Nonradial hydrodynamic instabilities in the collapsing stellar core, which can grow from small, random initial perturbations before neutrino heating revives the stalled shock, lead to low-multipole asymmetries that trigger anisotropic and inhomogeneous expulsion of matter. Hydrodynamic instabilities in the SN core therefore do not only yield a natural explanation of the origin of pulsar kicks up to more than 1000 km/s (Sect. VI A, Fig. 9); they also seed large-scale mixing processes in the exploding star, accounting for the penetration of high-velocity clumps of inner-core material into the hydrogen and helium ejecta of well observed SN explosions (Sect. VIB, Fig. 10).

First results of a systematic exploration of the progenitor-supernova connection based on the neutrino-heating mechanism show strong sensitivity of the explosion properties on the stellar structure and, for the employed set of stellar models [22], large variations even within narrow progenitor-mass intervals (Sect. VIC; Fig. 11). The explosion models can reproduce fundamental properties of the empirical remnant-mass distribution but reveal that neutrino-driven explosions are unlikely to explain SN energies above  $\sim 2 \times 10^{51}$  erg and nickel masses significantly higher than  $0.1 M_{\odot}$ . This underlines the need for an alternative engine that powers stellar blast waves with energies from several  $10^{51}$  erg up to more than  $10^{52}$  erg. Such hyperenergetic events, which typically also exhibit unusually large nickel ejection (Fig. 3) and deformation, are most probably energized by magnetorotational effects.

Many questions remain to be answered in this context and require more observations and theoretical work. What

discriminates progenitors of “normal” SNe from those of HNe? Is rapid rotation of the progenitors the crucial parameter? Is it connected to binary evolution? Is there a continuous spectrum of stellar explosions connecting the SN and HN regimes? Is a mixed mechanism, neutrino-heating in combination with magnetorotational energy transfer, at work in such events?

On the theory side the mission of clarifying the SN engines is severely handicapped by the unavailability of multi-dimensional stellar evolution models with the quality to reduce the major uncertainties of the stellar structure, rotation, and magnetic fields at the onset of core collapse. It is clear that reliable theoretical predictions of the progenitor-remnant connection and of explosion properties —energies, nucleosynthetic yields, asymmetries, remnant masses, and neutrino and GW signals— heavily depend on a firm knowledge of the stellar conditions at the time the gravitational instability is reached.

### Acknowledgments

Helpful discussions with P. Mazzali and A. Weiß are acknowledged. The author is very grateful to John Eldridge and Stephen Smartt for providing panel d of Fig. 3, to Mrs. Rosmarie Mayr-Ihbe for preparing Fig. 1, and to A. Marek, B. Müller, M. Ugliano, and A. Wongwathanarat for providing figures of their results from publications in preparation. Data from simulations by the Garching group are accessible either openly or upon request at <http://www.mpa-garching.mpg.de/ccsnarchive/>. This work was supported by the Deutsche Forschungsgemeinschaft through Sonderforschungsbereich/Transregio 27 “Neutrinos and Beyond”, Sonderforschungsbereich/Transregio 7 “Gravitational-Wave Astronomy”, and the Cluster of Excellence EXC 153 “Origin and Structure of the Universe”. Computing time at the John von Neumann Institute for Computing (NIC) in Jülich, the Höchstleistungsrechenzentrum (HLRS) of the University Stuttgart, the Rechenzentrum (RZG) Garching, and through DECI-5 and DECI-6 grants of the DEISA initiative of the EU FP7 are acknowledged.

Posted with permission from the Annual Review of Nuclear and Particle Science, Volume 62 © 2012 by Annual Reviews, <http://www.annualreviews.org>.

- 
- [1] E. M. Burbidge, G. R. Burbidge, W. A. Fowler, and F. Hoyle, *Reviews of Modern Physics* **29**, 547 (1957).
  - [2] W. Baade and F. Zwicky, *Physical Review* **46**, 76 (1934).
  - [3] F. Hoyle and W. A. Fowler, *Astrophys. J.* **132**, 565 (1960).
  - [4] S. A. Colgate and M. H. Johnson, *Physical Review Letters* **5**, 235 (1960).
  - [5] S. A. Colgate, W. H. Grasberger, and R. H. White, *Astronomical J.* **66**, 280 (1961).
  - [6] S. A. Colgate and R. H. White, *Astrophys. J.* **143**, 626 (1966).
  - [7] H. A. Bethe and J. R. Wilson, *Astrophys. J.* **295**, 14 (1985).
  - [8] M. Herant, W. Benz, W. R. Hix, C. L. Fryer, and S. A. Colgate, *Astrophys. J.* **435**, 339 (1994).
  - [9] A. Burrows, J. Hayes, and B. A. Fryxell, *Astrophys. J.* **450**, 830 (1995).
  - [10] H.-T. Janka and E. Müller, *Astrophys. J.* **448**, L109 (1995).
  - [11] H.-T. Janka and E. Müller, *Astron. Astrophys.* **306**, 167 (1996).
  - [12] C. L. Fryer, ed., *Stellar Collapse*, vol. 302 of *Astrophysics and Space Science Library* (2004).
  - [13] A. Mezzacappa, *Annual Review of Nuclear and Particle Science* **55**, 467 (2005).
  - [14] S. Woosley and H.-T. Janka, *Nature Physics* **1**, 147 (2005), [arXiv:astro-ph/0601261](https://arxiv.org/abs/astro-ph/0601261).
  - [15] S. E. Woosley and J. S. Bloom, *Ann. Rev. Astron. Astrophys.* **44**, 507 (2006), [arXiv:astro-ph/0609142](https://arxiv.org/abs/astro-ph/0609142).
  - [16] K. Kotake, K. Sato, and K. Takahashi, *Reports on Progress in Physics* **69**, 971 (2006), [arXiv:astro-ph/0509456](https://arxiv.org/abs/astro-ph/0509456).
  - [17] H.-T. Janka, K. Langanke, A. Marek, G. Martínez-Pinedo, and B. Müller, *Physics Reports* **442**, 38 (2007), [arXiv:astro-ph/0612072](https://arxiv.org/abs/astro-ph/0612072).
  - [18] C. D. Ott, *Classical and Quantum Gravity* **26**, 063001 (2009), 0809.0695.
  - [19] F.-K. Thielemann, R. Hirschi, M. Liebendörfer, and R. Diehl, in *Lecture Notes in Physics, Berlin Springer Verlag*, edited by R. Diehl, D. H. Hartmann, & N. Prantzos (2011), vol. 812 of *Lecture Notes in Physics, Berlin Springer Verlag*, pp. 153–232, 1008.2144.
  - [20] J. C. Wheeler, in *Supernovae, Jerusalem Winter School for Theoretical Physics*, edited by J. C. Wheeler, T. Piran, & S. Weinberg (1990), pp. 1–93.
  - [21] K. Nomoto, *Astrophys. J.* **277**, 791 (1984).
  - [22] S. E. Woosley, A. Heger, and T. A. Weaver, *Rev. Mod. Phys.* **74**, 1015 (2002).
  - [23] S. E. Woosley and T. A. Weaver, *Astrophys. J. Suppl.* **101**, 181 (1995).
  - [24] M. Tanaka, N. Tominaga, K. Nomoto, S. Valenti, D. K. Sahu, T. Minezaki, Y. Yoshii, M. Yoshida, G. C. Anupama, S. Benetti, et al., *Astrophys. J.* **692**, 1131 (2009), 0807.1674.
  - [25] V. P. Utrobin and N. N. Chugai, *Astron. Astrophys.* **532**, A100 (2011), 1107.2145.



- [26] S. J. Smartt, J. J. Eldridge, R. M. Crockett, and J. R. Maund, *Mon. Not. R. Astron. Soc.* **395**, 1409 (2009), 0809.0403.
- [27] S. J. Smartt, *Ann. Rev. Astron. Astrophys.* **47**, 63 (2009), 0908.0700.
- [28] K. Nomoto, *Astrophys. J.* **322**, 206 (1987).
- [29] A. J. T. Poelarends, F. Herwig, N. Langer, and A. Heger, *Astrophys. J.* **675**, 614 (2008), 0705.4643.
- [30] M. L. Pumo, M. Turatto, M. T. Botticella, A. Pastorello, S. Valenti, L. Zampieri, S. Benetti, E. Cappellaro, and F. Patat, *Astrophys. J.* **705**, L138 (2009), 0910.0640.
- [31] P. Podsiadlowski, N. Langer, A. J. T. Poelarends, S. Rappaport, A. Heger, and E. Pfahl, *Astrophys. J.* **612**, 1044 (2004), arXiv:astro-ph/0309588.
- [32] S. Wanajo, K. Nomoto, H.-T. Janka, F. S. Kitaura, and B. Müller, *Astrophys. J.* **695**, 208 (2009), 0810.3999.
- [33] S. Wanajo, H.-T. Janka, and B. Müller, *Astrophys. J.* **726**, L15 (2011), 1009.1000.
- [34] K. Nomoto, D. Sugimoto, W. M. Sparks, R. A. Fesen, T. R. Gull, and S. Miyaji, *Nature (London)* **299**, 803 (1982).
- [35] W. Hillebrandt, *Astron. Astrophys.* **110**, L3 (1982).
- [36] A. Heger, S. E. Woosley, and H. C. Spruit, *Astrophys. J.* **626**, 350 (2005), arXiv:astro-ph/0409422.
- [37] B. Paczynski, *Astrophys. J.* **494**, L45 (1998), arXiv:astro-ph/9710086.
- [38] K. Iwamoto, P. A. Mazzali, K. Nomoto, H. Umeda, T. Nakamura, F. Patat, I. J. Danziger, T. R. Young, T. Suzuki, T. Shigeyama, et al., *Nature (London)* **395**, 672 (1998), arXiv:astro-ph/9806382.
- [39] A. I. MacFadyen and S. E. Woosley, *Astrophys. J.* **524**, 262 (1999), arXiv:astro-ph/9810274.
- [40] R. Popham, S. E. Woosley, and C. Fryer, *Astrophys. J.* **518**, 356 (1999), arXiv:astro-ph/9807028.
- [41] S.-i. Fujimoto, N. Nishimura, and M.-a. Hashimoto, *Astrophys. J.* **680**, 1350 (2008), 0804.0969.
- [42] S.-C. Yoon and N. Langer, *Astron. Astrophys.* **443**, 643 (2005), arXiv:astro-ph/0508242.
- [43] S. E. Woosley and A. Heger, *Astrophys. J.* **637**, 914 (2006), arXiv:astro-ph/0508175.
- [44] A. Heger, C. L. Fryer, S. E. Woosley, N. Langer, and D. H. Hartmann, *Astrophys. J.* **591**, 288 (2003), arXiv:astro-ph/0212469.
- [45] S. E. Woosley and T. A. Weaver, in *NATO ASIC Proc. 90: Supernovae: A Survey of Current Research*, edited by M. J. Rees & R. J. Stoneham (1982), p. 79.
- [46] C. L. Fryer, S. E. Woosley, and A. Heger, *Astrophys. J.* **550**, 372 (2001).
- [47] N. Smith, W. Li, R. J. Foley, J. C. Wheeler, D. Pooley, R. Chornock, A. V. Filippenko, J. M. Silverman, R. Quimby, J. S. Bloom, et al., *Astrophys. J.* **666**, 1116 (2007), arXiv:astro-ph/0612617.
- [48] A. Gal-Yam, P. Mazzali, E. O. Ofek, P. E. Nugent, S. R. Kulkarni, M. M. Kasliwal, R. M. Quimby, A. V. Filippenko, S. B. Cenko, R. Chornock, et al., *Nature (London)* **462**, 624 (2009), 1001.1156.
- [49] S. E. Woosley, S. Blinnikov, and A. Heger, *Nature (London)* **450**, 390 (2007), 0710.3314.
- [50] D. Kasen and L. Bildsten, *Astrophys. J.* **717**, 245 (2010), 0911.0680.
- [51] A. Burrows and R. F. Sawyer, *Phys. Rev. C* **58**, 554 (1998).
- [52] C. J. Horowitz, *Phys. Rev. D* **65**, 043001 (2002), arXiv:astro-ph/0109209.
- [53] G. W. Carter and M. Prakash, *Physics Letters B* **525**, 249 (2002), arXiv:nucl-th/0106029.
- [54] S. Reddy, M. Prakash, J. M. Lattimer, and J. A. Pons, *Phys. Rev. C* **59**, 2888 (1999), arXiv:astro-ph/9811294.
- [55] K. Langanke, G. Martínez-Pinedo, J. M. Sampaio, D. J. Dean, W. R. Hix, O. E. Messer, A. Mezzacappa, M. Liebendörfer, H.-T. Janka, and M. Rampp, *Physical Review Letters* **90**, 241102 (2003), astro-ph/0302459.
- [56] C. J. Horowitz, *Phys. Rev. D* **55**, 4577 (1997).
- [57] K. Langanke, G. Martínez-Pinedo, B. Müller, H.-T. Janka, A. Marek, W. R. Hix, A. Juodagalvis, and J. M. Sampaio, *Phys. Rev. Lett.* **100**, 011101:1 (2008).
- [58] A. Mezzacappa and S. W. Bruenn, *Astrophys. J.* **405**, 669 (1993).
- [59] S. W. Bruenn, *Astrophys. J. Suppl.* **58**, 771 (1985).
- [60] J. A. Pons, J. A. Miralles, and J. M. A. Ibanez, *Astron. Astrophys. Suppl.* **129**, 343 (1998), arXiv:astro-ph/9802333.
- [61] S. Hannestad and G. Raffelt, *Astrophys. J.* **507**, 339 (1998).
- [62] R. Buras, H.-T. Janka, M. T. Keil, G. G. Raffelt, and M. Rampp, *Astrophys. J.* **587**, 320 (2003).
- [63] W. D. Arnett, *Canadian Journal of Physics* **44**, 2553 (1966).
- [64] J. R. Wilson, *Astrophys. J.* **163**, 209 (1971).
- [65] J. M. LeBlanc and J. R. Wilson, *Astrophys. J.* **161**, 541 (1970).
- [66] L. Smarr, J. R. Wilson, R. T. Barton, and R. L. Bowers, *Astrophys. J.* **246**, 515 (1981).
- [67] E. M. D. Symbalisty, *Astrophys. J.* **285**, 729 (1984).
- [68] R. Mönchmeyer, G. Schäfer, E. Müller, and R. E. Kates, *Astron. Astrophys.* **246**, 417 (1991).
- [69] W. D. Arnett, J. N. Bahcall, R. P. Kirshner, and S. E. Woosley, *Ann. Rev. Astron. Astrophys.* **27**, 629 (1989).
- [70] W. Hillebrandt and P. Höflich, *Reports on Progress in Physics* **52**, 1421 (1989).
- [71] J. R. Wilson and R. W. Mayle, *Physics Reports* **163**, 63 (1988).
- [72] S. W. Bruenn and T. Dineva, *Astrophys. J.* **458**, L71 (1996).
- [73] C. L. Fryer and M. S. Warren, *Astrophys. J.* **574**, L65 (2002), arXiv:astro-ph/0206017.
- [74] C. L. Fryer and M. S. Warren, *Astrophys. J.* **601**, 391 (2004), arXiv:astro-ph/0309539.
- [75] C. L. Fryer and P. A. Young, *Astrophys. J.* **659**, 1438 (2007), arXiv:astro-ph/0612154.
- [76] L. Scheck, H.-T. Janka, T. Foglizzo, and K. Kifonidis, *Astron. Astrophys.* **477**, 931 (2008), 0704.3001.
- [77] J. Sato, T. Foglizzo, and S. Fromang, *Astrophys. J.* **694**, 833 (2009), 0809.2303.
- [78] S. W. Bruenn, K. R. De Nisco, and A. Mezzacappa, *Astrophys. J.* **560**, 326 (2001).
- [79] E. J. Lentz, A. Mezzacappa, O. E. Bronson Messer, M. Liebendörfer, W. R. Hix, and S. W. Bruenn, *Astrophys. J.* **747**, 73 (2012), 1112.3595.

- [80] R. Buras, M. Rampp, H.-T. Janka, and K. Kifonidis, *Astron. Astrophys.* **447**, 1049 (2006).
- [81] B. Müller, H.-T. Janka, and A. Marek, eprint arXiv:1202.0815 (2012), 1202.0815.
- [82] J. M. Blondin and A. Mezzacappa, *Nature (London)* **445**, 58 (2007), arXiv:astro-ph/0611680.
- [83] R. Fernández, *Astrophys. J.* **725**, 1563 (2010), 1003.1730.
- [84] J. M. Blondin, A. Mezzacappa, and C. DeMarino, *Astrophys. J.* **584**, 971 (2003).
- [85] W. Iwakami, K. Kotake, N. Ohnishi, S. Yamada, and K. Sawada, *Astrophys. J.* **678**, 1207 (2008), 0710.2191.
- [86] W. Iwakami, K. Kotake, N. Ohnishi, S. Yamada, and K. Sawada, *Astrophys. J.* **700**, 232 (2009), 0811.0651.
- [87] J. Nordhaus, A. Burrows, A. Almgren, and J. Bell, *Astrophys. J.* **720**, 694 (2010), 1006.3792.
- [88] F. Hanke, A. Marek, B. Müller, and H.-T. Janka, *ArXiv e-prints* (2011), 1108.4355.
- [89] C. D. Ott, H. Dimmelfeier, A. Marek, H.-T. Janka, I. Hawke, B. Zink, and E. Schnetter, *Physical Review Letters* **98**, 261101 (2007), arXiv:astro-ph/0609819.
- [90] C. D. Ott, C. Reisswig, E. Schnetter, E. O'Connor, U. Sperhake, F. Löffler, P. Diener, E. Abdikamalov, I. Hawke, and A. Burrows, *Physical Review Letters* **106**, 161103 (2011), 1012.1853.
- [91] M. Rampp and H.-T. Janka, *Astron. Astrophys.* **396**, 361 (2002), arXiv:astro-ph/0203101.
- [92] A. Marek, H. Dimmelfeier, H.-T. Janka, E. Müller, and R. Buras, *Astron. Astrophys.* **445**, 273 (2006).
- [93] S. Scheidegger, R. Käppeli, S. C. Whitehouse, T. Fischer, and M. Liebendörfer, *Astron. Astrophys.* **514**, A51 (2010).
- [94] L. Scheck, K. Kifonidis, H.-T. Janka, and E. Müller, *Astron. Astrophys.* **457**, 963 (2006), arXiv:astro-ph/0601302.
- [95] A. Wongwathanarat, H. Janka, and E. Müller, *Astrophys. J.* **725**, L106 (2010), 1010.0167.
- [96] E. Müller, H.-T. Janka, and A. Wongwathanarat, *Astron. Astrophys.* **537**, A63 (2012), 1106.6301.
- [97] S. W. Bruenn, A. Mezzacappa, W. R. Hix, J. M. Blondin, P. Marronetti, O. E. B. Messer, C. J. Dirk, and S. Yoshida, *Journal of Physics Conference Series* **180**, 012018 (2009).
- [98] T. Takiwaki, K. Kotake, and Y. Suwa, *Astrophys. J.* **749**, 98 (2012), 1108.3989.
- [99] M. Liebendörfer, T. Fischer, M. Hempel, R. Käppeli, G. Pagliara, A. Perego, I. Sagert, J. Schaffner-Bielich, S. Scheidegger, F. Thielemann, et al., *Progress of Theoretical Physics Supplement* **186**, 87 (2010).
- [100] S. Yamada, H.-T. Janka, and H. Suzuki, *Astron. Astrophys.* **344**, 533 (1999).
- [101] M. Liebendörfer, O. E. B. Messer, A. Mezzacappa, S. W. Bruenn, C. Y. Cardall, and F.-K. Thielemann, *Astrophys. J. Suppl.* **150**, 263 (2004).
- [102] A. Burrows, T. Young, P. Pinto, R. Eastman, and T. A. Thompson, *Astrophys. J.* **539**, 865 (2000), arXiv:astro-ph/9905132.
- [103] B. Müller, H.-T. Janka, and H. Dimmelfeier, *Astrophys. J. Suppl.* **189**, 104 (2010), 1001.4841.
- [104] R. Buras, H.-T. Janka, M. Rampp, and K. Kifonidis, *Astron. Astrophys.* **457**, 281 (2006).
- [105] F. S. Kitaura, H.-T. Janka, and W. Hillebrandt, *Astron. Astrophys.* **450**, 345 (2006).
- [106] A. Marek and H.-T. Janka, *Astrophys. J.* **694**, 664 (2009), 0708.3372.
- [107] L. Hüdepohl, B. Müller, H.-T. Janka, A. Marek, and G. G. Raffelt, *Physical Review Letters* **104**, 251101 (2010), 0912.0260.
- [108] A. Burrows, E. Livne, L. Dessart, C. D. Ott, and J. Murphy, *Astrophys. J.* **640**, 878 (2006).
- [109] A. Burrows, E. Livne, L. Dessart, C. D. Ott, and J. Murphy, *Astrophys. J.* **655**, 416 (2007), arXiv:astro-ph/0610175.
- [110] A. Burrows, L. Dessart, E. Livne, C. D. Ott, and J. Murphy, *Astrophys. J.* **664**, 416 (2007), arXiv:astro-ph/0702539.
- [111] C. D. Ott, A. Burrows, L. Dessart, and E. Livne, *Astrophys. J.* **685**, 1069 (2008), 0804.0239.
- [112] T. D. Brandt, A. Burrows, C. D. Ott, and E. Livne, *Astrophys. J.* **728**, 8 (2011), 1009.4654.
- [113] F. D. Swesty and E. S. Myra, *Astrophys. J. Suppl.* **181**, 1 (2009).
- [114] M. Obergaulinger and H.-T. Janka, *ArXiv e-prints* (2011), 1101.1198.
- [115] M. Liebendörfer, S. C. Whitehouse, and T. Fischer, *Astrophys. J.* **698**, 1174 (2009).
- [116] Y. Suwa, K. Kotake, T. Takiwaki, S. C. Whitehouse, M. Liebendörfer, and K. Sato, *Publ. Astron. Soc. Japan* **62**, L49 (2010), 0912.1157.
- [117] K. Sumiyoshi and S. Yamada, *Astrophys. J. Suppl.* **199**, 17 (2012), 1201.2244.
- [118] S. Bonazzola and N. Vasset, *ArXiv e-prints* (2011), 1104.5330.
- [119] M. Shibata, K. Kiuchi, Y. Sekiguchi, and Y. Suwa, *Progress of Theoretical Physics* **125**, 1255 (2011), 1104.3937.
- [120] M. Liebendörfer, M. Rampp, H.-T. Janka, and A. Mezzacappa, *Astrophys. J.* **620**, 840 (2005).
- [121] A. Marek and H.-T. Janka, in preparation (2012).
- [122] W. Hillebrandt, K. Nomoto, and R. G. Wolff, *Astron. Astrophys.* **133**, 175 (1984).
- [123] K. Hebel, J. M. Lattimer, C. J. Pethick, and A. Schwenk, *Physical Review Letters* **105**, 161102 (2010), 1007.1746.
- [124] P. B. Demorest, T. Pennucci, S. M. Ransom, M. S. E. Roberts, and J. W. T. Hessels, *Nature (London)* **467**, 1081 (2010), 1010.5788.
- [125] J. M. Lattimer and M. Prakash, *ArXiv e-prints* (2010), 1012.3208.
- [126] A. W. Steiner, J. M. Lattimer, and E. F. Brown, *Astrophys. J.* **722**, 33 (2010), 1005.0811.
- [127] J. M. Lattimer and F. D. Swesty, *Nucl. Phys. A* **535**, 331 (1991).
- [128] H. Shen, H. Toki, K. Oyamatsu, and K. Sumiyoshi, *Nucl. Phys. A* **637**, 435 (1998).
- [129] J. M. Lattimer, C. J. Pethick, D. G. Ravenhall, and D. Q. Lamb, *Nuclear Physics A* **432**, 646 (1985).
- [130] H.-T. Janka, R. Buras, F. S. Kitaura Joyanes, A. Marek, M. Rampp, and L. Scheck, *Nuclear Physics A* **758**, 19 (2005), arXiv:astro-ph/0411347.
- [131] E. Lentz, W. R. Hix, M. L. Baird, O. E. B. Messer, and A. Mezzacappa, in *Nuclei in the Cosmos*. (2010), 1101.0156.
- [132] M. Hempel, T. Fischer, J. Schaffner-Bielich, and M. Liebendörfer, *Astrophys. J.* **748**, 70 (2012), 1108.0848.
- [133] J. M. Lattimer and M. Prakash, *Physics Reports* **333**, 121 (2000), arXiv:astro-ph/0002203.
- [134] S. Shlomo, V. M. Kolomietz, and G. Colò, *European Physical Journal A* **30**, 23 (2006).



- [135] J. Piekarewicz, Journal of Physics G Nuclear Physics **37**, 064038 (2010), 0912.5103.
- [136] F. D. Swesty, J. M. Lattimer, and E. S. Myra, Astrophys. J. **425**, 195 (1994).
- [137] T. A. Thompson, A. Burrows, and P. A. Pinto, Astrophys. J. **592**, 434 (2003), arXiv:astro-ph/0211194.
- [138] L. F. Roberts, G. Shen, V. Cirigliano, J. A. Pons, S. Reddy, and S. E. Woosley, Physical Review Letters, vol. 108, Issue 6, id. 061103 **108**, 061103 (2012), 1112.0335.
- [139] M. Hempel and J. Schaffner-Bielich, Nuclear Physics A **837**, 210 (2010), 0911.4073.
- [140] G. Shen, C. J. Horowitz, and S. Teige, Phys. Rev. C **83**, 035802 (2011), 1101.3715.
- [141] G. Shen, C. J. Horowitz, and E. O'Connor, Phys. Rev. C **83**, 065808 (2011), 1103.5174.
- [142] H. Shen, H. Toki, K. Oyamatsu, and K. Sumiyoshi, Astrophys. J. Suppl. **197**, 20 (2011), 1105.1666.
- [143] K. Sumiyoshi and G. Röpke, Phys. Rev. C **77**, 055804 (2008), 0801.0110.
- [144] S. Typel, G. Röpke, T. Klähn, D. Blaschke, and H. H. Wolter, Phys. Rev. C **81**, 015803 (2010), 0908.2344.
- [145] M. Hempel, J. Schaffner-Bielich, S. Typel, and G. Röpke, Phys. Rev. C **84**, 055804 (2011), 1109.0252.
- [146] A. Arcones, G. Martínez-Pinedo, E. O'Connor, A. Schwenk, H.-T. Janka, C. J. Horowitz, and K. Langanke, Phys. Rev. C **78**, 015806 (2008), 0805.3752.
- [147] B. Müller, H.-T. Janka, A. Marek, F. Hanke, A. Wongwathanarat, and E. Müller, ArXiv e-prints (2011), 1112.1913.
- [148] S. S. Gershtein, V. S. Imshennik, D. K. Nadezhin, V. N. Folomeshkin, M. I. Khlopov, V. M. Chechetkin, and R. A. Eramzhian, Zhurnal Eksperimental'noi i Teoreticheskoi Fiziki **69**, 1473 (1976).
- [149] V. M. Chechetkin, R. A. Eramzhyan, V. N. Folomeshkin, S. S. Gerstein, V. S. Imshennik, M. Y. Khlopov, and D. K. Nadyozhin, Physics Letters B **62**, 100 (1976).
- [150] N. V. Zmitrenko, V. S. Imshennik, M. I. Khlopov, and V. M. Chechetkin, Zhurnal Eksperimental'noi i Teoreticheskoi Fiziki **75**, 1169 (1978).
- [151] V. M. Chechetkin, S. S. Gershtein, V. S. Imshennik, L. N. Ivanova, and M. I. Khlopov, Astrophysics and Space Science **67**, 61 (1980).
- [152] H. A. Bethe, Rev. Mod. Phys. **62**, 801 (1990).
- [153] T. J. Mazurek, Astrophys. J. **259**, L13 (1982).
- [154] W. R. Hix, O. E. Messer, A. Mezzacappa, M. Liebendörfer, J. Sampaio, K. Langanke, D. J. Dean, and G. Martínez-Pinedo, Physical Review Letters **91**, 201102 (2003), arXiv:astro-ph/0310883.
- [155] H.-T. Janka, Astron. Astrophys. **368**, 527 (2001).
- [156] T. Foglizzo, L. Scheck, and H.-T. Janka, Astrophys. J. **652**, 1436 (2006), arXiv:astro-ph/0507636.
- [157] H.-T. Janka, K. Kifonidis, and M. Rampp, in *Physics of Neutron Star Interiors*, edited by D. Blaschke, N. K. Glendenning, & A. Sedrakian (2001), vol. 578 of *Lecture Notes in Physics, Berlin Springer Verlag*, p. 333.
- [158] H.-T. Janka and W. Keil, in *Supernovae and cosmology*, edited by L. Labhardt, B. Binggeli, & R. Buser (1998), p. 7, arXiv:astro-ph/9709012.
- [159] H.-T. Janka, B. Müller, F. S. Kitaura, and R. Buras, Astron. Astrophys. **485**, 199 (2008).
- [160] T. Fischer, S. C. Whitehouse, A. Mezzacappa, F.-K. Thielemann, and M. Liebendörfer, Astron. Astrophys. **517**, A80 (2010), 0908.1871.
- [161] B. Müller, H.-T. Janka, and A. Heger, eprint arXiv:1205.7078 (2012), 1205.7078.
- [162] C. D. Ott, E. P. O'Connor, and B. Dasgupta, ArXiv e-prints (2011), 1111.6282.
- [163] S. Chakraborty, T. Fischer, A. Mirizzi, N. Saviano, and R. Tomàs, Physical Review Letters **107**, 151101 (2011), 1104.4031.
- [164] S. Chakraborty, T. Fischer, A. Mirizzi, N. Saviano, and R. Tomàs, Phys. Rev. D **84**, 025002 (2011), 1105.1130.
- [165] B. Dasgupta, E. P. O'Connor, and C. D. Ott, Phys. Rev. D **85**, 065008 (2012), 1106.1167.
- [166] S. Sarikas, G. G. Raffelt, L. Hudepohl, and H.-T. Janka, Physical Review Letters, vol. 108, Issue 6, id. 061101 **108**, 061101 (2012), 1109.3601.
- [167] J. W. Murphy and A. Burrows, Astrophys. J. **688**, 1159 (2008), 0805.3345.
- [168] J. M. Blondin and A. Mezzacappa, Astrophys. J. **642**, 401 (2006).
- [169] N. Ohnishi, K. Kotake, and S. Yamada, Astrophys. J. **641**, 1018 (2006), arXiv:astro-ph/0509765.
- [170] T. Foglizzo, P. Galletti, L. Scheck, and H.-T. Janka, Astrophys. J. **654**, 1006 (2007).
- [171] J. Guilet and T. Foglizzo, Mon. Not. R. Astron. Soc. **421**, 546 (2012), 1112.1427.
- [172] T. Foglizzo, F. Masset, J. Guilet, and G. Durand, Physical Review Letters, vol. 108, Issue 5, id. 051103 **108**, 051103 (2012), 1112.3448.
- [173] T. Foglizzo, Astron. Astrophys. **368**, 311 (2001).
- [174] T. Foglizzo, Astron. Astrophys. **392**, 353 (2002).
- [175] A. Burrows and J. Goshy, Astrophys. J. **416**, L75 (1993).
- [176] T. Yamasaki and S. Yamada, Astrophys. J. **623**, 1000 (2005), arXiv:astro-ph/0412625.
- [177] T. Yamasaki and S. Yamada, Astrophys. J. **650**, 291 (2006), arXiv:astro-ph/0606504.
- [178] O. Pejcha and T. A. Thompson, Astrophys. J. **746**, 106 (2012), 1103.4864.
- [179] R. Fernández, Astrophys. J. **749**, 142 (2012), 1111.0665.
- [180] T. A. Thompson, E. Quataert, and A. Burrows, Astrophys. J. **620**, 861 (2005).
- [181] J. W. Murphy and C. Meakin, Astrophys. J. **742**, 74 (2011), 1106.5496.
- [182] T. Yamasaki and S. Yamada, Astrophys. J. **656**, 1019 (2007), arXiv:astro-ph/0606581.
- [183] R. Fernández and C. Thompson, Astrophys. J. **703**, 1464 (2009), 0812.4574.
- [184] T. Yamasaki and T. Foglizzo, Astrophys. J. **679**, 607 (2008), 0710.3041.
- [185] A. Burrows, J. C. Dolence, and J. W. Murphy, eprint arXiv:1204.3088 (2012), 1204.3088.
- [186] J. W. Murphy, J. C. Dolence, and A. Burrows, eprint arXiv:1205.3491 (2012), 1205.3491.

- [187] G. S. Bisnovatyi-Kogan, *Astronomicheskii Zhurnal* **47**, 813 (1970).
- [188] J. P. Ostriker and J. E. Gunn, *Astrophys. J.* **164**, L95 (1971).
- [189] D. L. Meier, R. I. Epstein, W. D. Arnett, and D. N. Schramm, *Astrophys. J.* **204**, 869 (1976).
- [190] G. S. Bisnovatyi-Kogan, I. P. Popov, and A. A. Samokhin, *Astrophysics and Space Science* **41**, 287 (1976).
- [191] K. Kotake, H. Sawai, S. Yamada, and K. Sato, *Astrophys. J.* **608**, 391 (2004).
- [192] H. Sawai, K. Kotake, and S. Yamada, *Astrophys. J.* **631**, 446 (2005), arXiv:astro-ph/0505611.
- [193] M. Obergaulinger, M. A. Aloy, H. Dimmellemeier, and E. Müller, *Astron. Astrophys.* **457**, 209 (2006), arXiv:astro-ph/0602187.
- [194] S. G. Moiseenko, G. S. Bisnovatyi-Kogan, and N. V. Ardeljan, *Mon. Not. R. Astron. Soc.* **370**, 501 (2006).
- [195] S. A. Balbus and J. F. Hawley, *Reviews of Modern Physics* **70**, 1 (1998).
- [196] S. Akiyama, J. C. Wheeler, D. L. Meier, and I. Lichtenstadt, *Astrophys. J.* **584**, 954 (2003), arXiv:astro-ph/0208128.
- [197] M. Obergaulinger, P. Cerdá-Durán, E. Müller, and M. A. Aloy, *Astron. Astrophys.* **498**, 241 (2009), 0811.1652.
- [198] J. C. Wheeler, D. L. Meier, and J. R. Wilson, *Astrophys. J.* **568**, 807 (2002), arXiv:astro-ph/0112020.
- [199] S. Charpinet, G. Fontaine, and P. Brassard, *Nature (London)* **461**, 501 (2009).
- [200] G. Meynet, P. Eggenberger, and A. Maeder, *Astron. Astrophys.* **525**, L11 (2011), 1011.5795.
- [201] C. Thompson and R. C. Duncan, *Astrophys. J.* **408**, 194 (1993).
- [202] E. Endeve, C. Y. Cardall, R. D. Budiardja, and A. Mezzacappa, *Astrophys. J.* **713**, 1219 (2010), 0811.3385.
- [203] J. Guilet, T. Foglizzo, and S. Fromang, *Astrophys. J.* **729**, 71 (2011), 1006.4697.
- [204] T. K. Suzuki, K. Sumiyoshi, and S. Yamada, *Astrophys. J.* **678**, 1200 (2008), 0707.4345.
- [205] A. Burrows, L. Dessart, C. D. Ott, and E. Livne, *Physics Reports* **442**, 23 (2007), arXiv:astro-ph/0612460.
- [206] N. N. Weinberg and E. Quataert, *Mon. Not. R. Astron. Soc.* **387**, L64 (2008), 0802.1522.
- [207] I. Sagert, T. Fischer, M. Hempel, G. Pagliara, J. Schaffner-Bielich, A. Mezzacappa, F.-K. Thielemann, and M. Liebendörfer, *Physical Review Letters* **102**, 081101 (2009), 0809.4225.
- [208] T. Fischer, I. Sagert, G. Pagliara, M. Hempel, J. Schaffner-Bielich, T. Rauscher, F.-K. Thielemann, R. Käppeli, G. Martínez-Pinedo, and M. Liebendörfer, *Astrophys. J. Suppl.* **194**, 39 (2011), 1011.3409.
- [209] M. Prakash, J. R. Cooke, and J. M. Lattimer, *Phys. Rev. D* **52**, 661 (1995).
- [210] T. Fischer, D. Blaschke, M. Hempel, T. Klähn, R. Łastowiecki, M. Liebendörfer, G. Martínez-Pinedo, G. Pagliara, I. Sagert, F. Sandin, et al., *ArXiv e-prints* (2011), 1103.3004.
- [211] B. Dasgupta, T. Fischer, S. Horiuchi, M. Liebendörfer, A. Mirizzi, I. Sagert, and J. Schaffner-Bielich, *Phys. Rev. D* **81**, 103005 (2010), 0912.2568.
- [212] K. Sumiyoshi, S. Yamada, and H. Suzuki, *Astrophys. J.* **688**, 1176 (2008), 0808.0384.
- [213] T. Fischer, S. C. Whitehouse, A. Mezzacappa, F.-K. Thielemann, and M. Liebendörfer, *Astron. Astrophys.* **499**, 1 (2009), 0809.5129.
- [214] A. Marek, H.-T. Janka, and E. Müller, *Astron. Astrophys.* **496**, 475 (2009), 0808.4136.
- [215] T. Lund, A. Marek, C. Lunardini, H.-T. Janka, and G. Raffelt, *Phys. Rev. D* **82**, 063007 (2010), 1006.1889.
- [216] T. Fischer, G. Martínez-Pinedo, M. Hempel, and M. Liebendörfer, *Phys. Rev. D* **85**, 083003 (2012), 1112.3842.
- [217] L. F. Roberts, eprint arXiv:1205.3228 (2012), 1205.3228.
- [218] L. F. Roberts and S. Reddy, eprint arXiv:1205.4066 (2012), 1205.4066.
- [219] G. Martínez-Pinedo, T. Fischer, A. Lohs, and L. Huther, eprint arXiv:1205.2793 (2012), 1205.2793.
- [220] T. A. Thompson, A. Burrows, and J. E. Horvath, *Phys. Rev. C* **62**, 035802 (2000), arXiv:astro-ph/0003054.
- [221] M. T. Keil, G. G. Raffelt, and H.-T. Janka, *Astrophys. J.* **590**, 971 (2003), arXiv:astro-ph/0208035.
- [222] G. G. Raffelt, *Astrophys. J.* **561**, 890 (2001), arXiv:astro-ph/0105250.
- [223] D. L. Tubbs, *Astrophys. J.* **231**, 846 (1979).
- [224] P. D. Serpico, S. Chakraborty, T. Fischer, L. Hüdepohl, H.-T. Janka, and A. Mirizzi, *Phys. Rev. D* **85**, 085031 (2012), 1111.4483.
- [225] P. Banerjee, W. C. Haxton, and Y.-Z. Qian, *Physical Review Letters* **106**, 201104 (2011), 1103.1193.
- [226] H. Duan, A. Friedland, G. C. McLaughlin, and R. Surman, *Journal of Physics G Nuclear Physics* **38**, 035201 (2011), 1012.0532.
- [227] J. W. Murphy, C. D. Ott, and A. Burrows, *Astrophys. J.* **707**, 1173 (2009), 0907.4762.
- [228] C. D. Ott, A. Burrows, L. Dessart, and E. Livne, *Physical Review Letters* **96**, 201102 (2006), arXiv:astro-ph/0605493.
- [229] K. Kotake, W. Iwakami, N. Ohnishi, and S. Yamada, *Astrophys. J.* **697**, L133 (2009), 0904.4300.
- [230] K. Kotake, *ArXiv e-prints* (2011), 1110.5107.
- [231] Y.-Z. Qian and S. E. Woosley, *Astrophys. J.* **471**, 331 (1996), arXiv:astro-ph/9611094.
- [232] T. A. Thompson, A. Burrows, and B. S. Meyer, *Astrophys. J.* **562**, 887 (2001), arXiv:astro-ph/0105004.
- [233] R. D. Hoffman, S. E. Woosley, and Y.-Z. Qian, *Astrophys. J.* **482**, 951 (1997), arXiv:astro-ph/9611097.
- [234] K. Takahashi, J. Witt, and H.-T. Janka, *Astron. Astrophys.* **286**, 857 (1994).
- [235] L. F. Roberts, S. E. Woosley, and R. D. Hoffman, *Astrophys. J.* **722**, 954 (2010), 1004.4916.
- [236] C. Fröhlich, G. Martínez-Pinedo, M. Liebendörfer, F.-K. Thielemann, E. Bravo, W. R. Hix, K. Langanke, and N. T. Zinner, *Physical Review Letters* **96**, 142502 (2006), arXiv:astro-ph/0511376.
- [237] J. Pruet, R. D. Hoffman, S. E. Woosley, H.-T. Janka, and R. Buras, *Astrophys. J.* **644**, 1028 (2006), arXiv:astro-ph/0511194.
- [238] I. Tamborra, G. G. Raffelt, L. Hüdepohl, and H.-T. Janka, *JCAP* **1**, 13 (2012), 1110.2104.
- [239] A. Wongwathanarat, H.-T. Janka, and E. Müller, in preparation (2012).
- [240] N. J. Hammer, H.-T. Janka, and E. Müller, *Astrophys. J.* **714**, 1371 (2010), 0908.3474.

- [241] M. Ugliano, H.-T. Janka, A. Marek, and A. Arcones, eprint arXiv:1205.3657 (2012), 1205.3657.
- [242] G. Hobbs, D. R. Lorimer, A. G. Lyne, and M. Kramer, *Mon. Not. R. Astron. Soc.* **360**, 974 (2005), arXiv:astro-ph/0504584.
- [243] D. Lai, D. F. Chernoff, and J. M. Cordes, *Astrophys. J.* **549**, 1111 (2001), arXiv:astro-ph/0007272.
- [244] H.-T. Janka and E. Müller, *Astron. Astrophys.* **290**, 496 (1994).
- [245] A. Burrows and J. Hayes, *Physical Review Letters* **76**, 352 (1996), arXiv:astro-ph/9511106.
- [246] W. D. Arnett and C. Meakin, *Astrophys. J.* **733**, 78 (2011), 1101.5646.
- [247] A. Kusenko, B. P. Mandal, and A. Mukherjee, *Phys. Rev. D* **77**, 123009 (2008), 0801.4734.
- [248] L. Scheck, T. Plewa, H.-T. Janka, K. Kifonidis, and E. Müller, *Physical Review Letters* **92**, 011103 (2004), arXiv:astro-ph/0307352.
- [249] J. Nordhaus, T. D. Brandt, A. Burrows, E. Livne, and C. D. Ott, *Phys. Rev. D* **82**, 103016 (2010), 1010.0674.
- [250] J. Nordhaus, T. Brandt, A. Burrows, and A. Almgren, *ArXiv e-prints* (2011), 1112.3342.
- [251] E. Rantsiou, A. Burrows, J. Nordhaus, and A. Almgren, *Astrophys. J.* **732**, 57 (2011), 1010.5238.
- [252] C. D. Ott, A. Burrows, T. A. Thompson, E. Livne, and R. Walder, *Astrophys. J. Suppl.* **164**, 130 (2006), arXiv:astro-ph/0508462.
- [253] K. Kifonidis, T. Plewa, H.-T. Janka, and E. Müller, *Astron. Astrophys.* **408**, 621 (2003), arXiv:astro-ph/0302239.
- [254] K. Kifonidis, T. Plewa, L. Scheck, H.-T. Janka, and E. Müller, *Astron. Astrophys.* **453**, 661 (2006), arXiv:astro-ph/0511369.
- [255] J. Casares, in *IAU Symposium*, edited by V. Karas & G. Matt (2007), vol. 238 of *IAU Symposium*, pp. 3–12, arXiv:astro-ph/0612312.
- [256] J. Ziolkowski, *Mem. S. A. It.* **81**, 294 (2010).
- [257] K. Belczynski, G. Wiktorowicz, C. Fryer, D. Holz, and V. Kalogera, *ArXiv e-prints* (2011), 1110.1635.
- [258] C. L. Fryer, K. Belczynski, G. Wiktorowicz, M. Dominik, V. Kalogera, and D. E. Holz, *Astrophys. J.* **749**, 91 (2012), 1110.1726.
- [259] W. Zhang, S. E. Woosley, and A. Heger, *Astrophys. J.* **679**, 639 (2008), arXiv:astro-ph/0701083.
- [260] E. O'Connor and C. D. Ott, *Astrophys. J.* **730**, 70 (2011), 1010.5550.
- [261] O. Pejcha, T. A. Thompson, and C. S. Kochanek, eprint arXiv:1204.5478 (2012), 1204.5478.
- [262] M. Kachelrieß, R. Tomàs, R. Buras, H.-T. Janka, A. Marek, and M. Rampp, *Phys. Rev. D* **71**, 063003 (2005), arXiv:astro-ph/0412082.
- [263] J. Ellis, H.-T. Janka, N. E. Mavromatos, A. S. Sakharov, and E. K. G. Sarkisyan, *Phys. Rev. D* **85**, 045032 (2012), 1110.4848.
- [264] J. Ellis, H.-T. Janka, N. E. Mavromatos, A. S. Sakharov, and E. K. G. Sarkisyan, eprint arXiv:1202.0248 (2012), 1202.0248.